### Title

Application of a high-throughput analyzer in evaluating solid adsorbents for post-combustion carbon capture via multicomponent adsorption of CO2, N2, and H2O.




### Journal

Journal of the American Chemical Society, 137(14)

### ISSN

0002-7863



### Authors

Mason, Jarad A
McDonald, Thomas M
Bae, Tae-Hyun
et al.



### Publication Date

2015-04-01

### DOI

10.1021/jacs.5b00838

Peer reviewed

JACS
JOURNAL OF THE AMERICAN CHEMICAL SOCIETY

Article

pubs.acs.org/JACS

# Application of a High-Throughput Analyzer in Evaluating Solid Adsorbents for Post-Combustion Carbon Capture via Multicomponent Adsorption of $CO_2$, $N_2$, and $H_2O$

Jarad A. Mason,[†] Thomas M. McDonald,[†] Tae-Hyun Bae,[†,§] Jonathan E. Bachman,[†] Kenji Sumida,[†,⊥] Justin J. Dutton,[‡] Steven S. Kaye,[‡,∥] and Jeffrey R. Long*[,†]

[†]Department of Chemistry, University of California, Berkeley and Materials Science Division, Lawrence Berkeley National Laboratory, Berkeley, California 94720, United States

[‡]Wildcat Discovery Technologies Inc., San Diego, California 92121, United States

Supporting Information

**ABSTRACT:** Despite the large number of metal−organic frameworks that have been studied in the context of post-combustion carbon capture, adsorption equilibria of gas mixtures including $CO_2$, $N_2$, and $H_2O$, which are the three biggest components of the flue gas emanating from a coal- or natural gas-fired power plant, have never been reported. Here, we disclose the design and validation of a high-throughput multicomponent adsorption instrument that can measure equilibrium adsorption isotherms for mixtures of gases at conditions that are representative of an actual flue gas from a power plant. This instrument is used to study 15 different metal−organic frameworks, zeolites, mesoporous silicas, and activated carbons representative of the broad range of solid adsorbents that have received attention for $CO_2$ capture. While the multicomponent results presented in this work provide many interesting fundamental insights, only adsorbents functionalized with alkylamines are shown to have any significant $CO_2$ capacity in the presence of $N_2$ and $H_2O$ at equilibrium partial pressures similar to those expected in a carbon capture process. Most significantly, the amine-appended metal organic framework mmen-$Mg_2$(dobpdc) (mmen = *N*,*N*′-dimethylethylenediamine, dobpdc $^{4-}$ = 4,4′-dioxido-3,3′-biphenyldicarboxylate) exhibits a record $CO_2$ capacity of 4.2 ± 0.2 mmol/g (16 wt %) at 0.1 bar and 40 °C in the presence of a high partial pressure of $H_2O$.

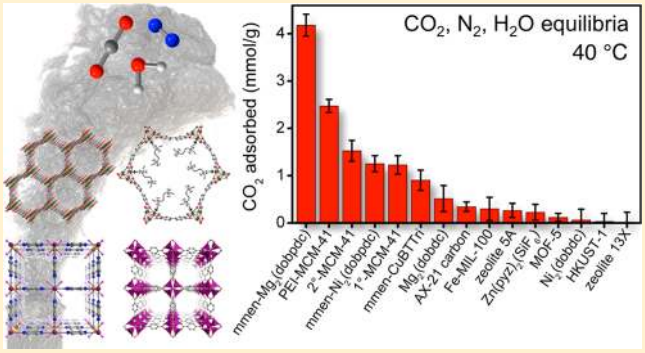


## INTRODUCTION

In 2012, coal- and natural gas-fired power plants released 11.1 Gt of carbon dioxide—nearly 30% of the total global emissions.[1,2] While there are more than 68,000 power plants currently in operation, approximately 300 of these plants are directly responsible for an astonishing 10% of the world's $CO_2$ emissions. Capturing and permanently sequestering this $CO_2$ would have a significant and immediate impact on rising levels of $CO_2$ in the atmosphere.[3,4] With little financial incentive to reduce $CO_2$ emissions in most countries, however, existing carbon capture technologies are simply too expensive to be practical at the scales required for large power plants that release upward of 40 tonnes of $CO_2$ per minute.[4,5] Since the most expensive component of any carbon capture and sequestration process is the separation of $CO_2$ from the other gases present in the flue gas of a power plant, a large research effort has focused on developing new materials and processes to remove $CO_2$ from flue gas using as little energy as possible.[6,7] While the exact composition of a flue gas depends on the design of the power plant and the source of natural gas or coal, a mixture of mostly $N_2$, $CO_2$, and $H_2O$ is released at ambient pressure and 40−80 °C (Table 1).[8] The effects of potentially more reactive gases that are present in lower concentrations, such as $O_2$, $SO_x$, $NO_x$, and CO, must also be considered, but, at a minimum, materials are needed that can selectively capture a large amount of $CO_2$ in the presence of $N_2$ and $H_2O$.

**Table 1. Expected Range of Compositions for Flue Gas From a Coal- or Natural Gas-Fired Power Plant[8]**

| | coal | natural gas |
|---|---|---|
| $CO_2$ (mbar) | 120−150 | 30−50 |
| $N_2$ (mbar) | 750−800 | 740−800 |
| $H_2O$ (mbar)[9] | 50−140 | 70−100 |

Taking advantage of the Lewis acidity of $CO_2$, Lewis basic aqueous amine solutions have been studied extensively for extracting $CO_2$ from gas mixtures and are currently used to remove $CO_2$ from many natural gas streams around the

**Received:** January 25, 2015
**Published:** April 6, 2015





DOI: 10.1021/jacs.5b00838
J. Am. Chem. Soc. 2015, 137, 4787−4803

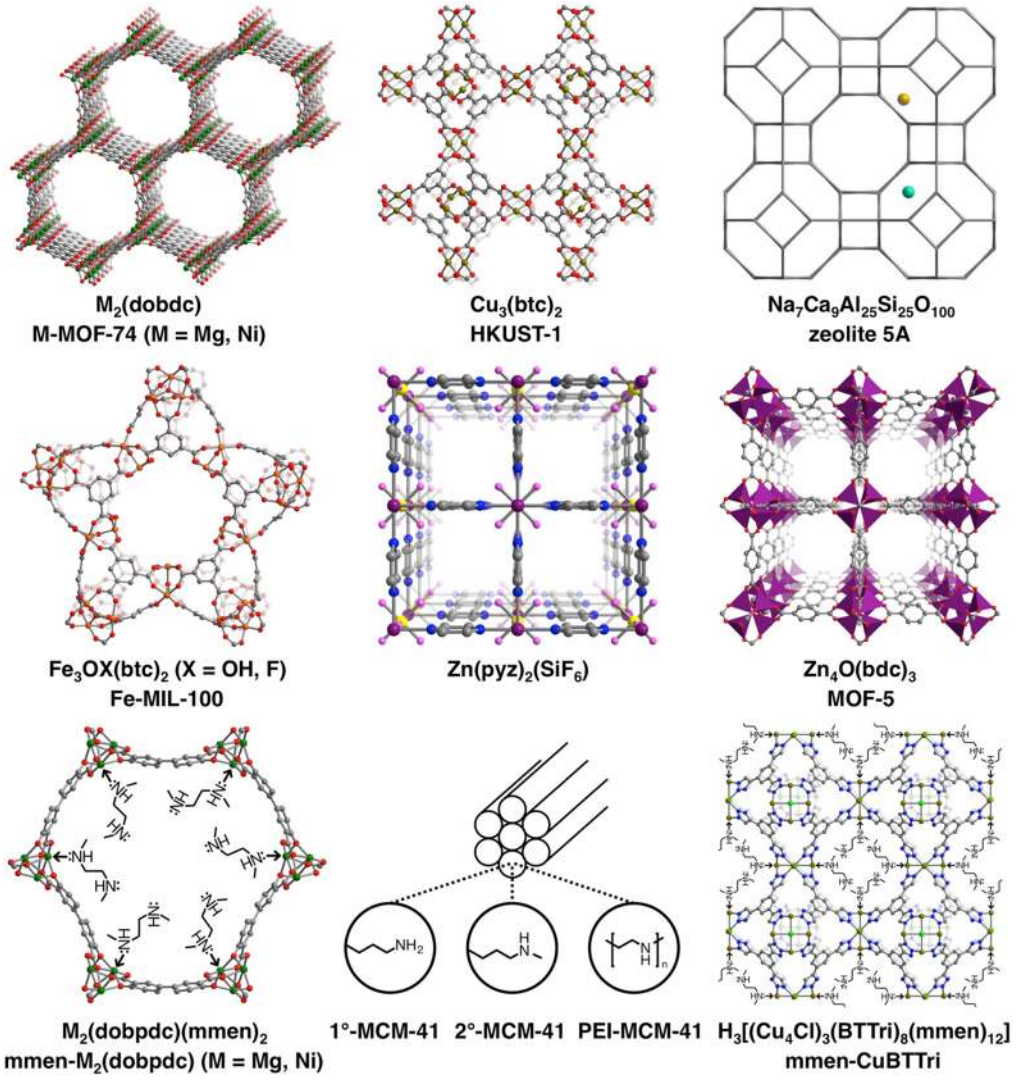


**Figure 1.** Multicomponent adsorption measurements were performed for mixtures of $CO_2$, $N_2$, and $H_2O$ in all of the adsorbents shown above as well as zeolite 13X ($Na_{50}Al_{50}Si_{59}O_{218}$) and an activated carbon (AX-21) that are not pictured. For the metal–organic framework structures, gray, red, blue, dark-yellow, orange, purple, pink, yellow, and bright-green spheres represent C, O, N, Cu, Fe, Zn, F, Si, and Cl atoms, respectively; H atoms have been omitted for clarity. Purple tetrahedra represent Zn atoms, and dark-green spheres represent Mg or Ni atoms. For the zeolite structure (upper right), each vertex represents a tetrahedral $SiO_4$ or $AlO_4$ unit, while teal and dark-orange spheres represent typical positions for extra-framework Na and Ca cations, respectively.

world.[10] Aqueous amine scrubbers can also be used to capture high-purity $CO_2$ from flue gas, but new materials with lower regeneration energy requirements could lead to a significantly lower overall cost for carbon capture.

To this end, solid adsorbents, including zeolites, activated carbons, silicas, and metal–organic frameworks, have received significant attention as alternatives to amine solutions, demonstrating high $CO_2$ capacities and high selectivities for $CO_2$ over $N_2$, together with reduced regeneration energy penalties.[11] It is now well established that adsorbents must contain strong $CO_2$ binding sites in order to adsorb a significant amount of $CO_2$ at 50–150 mbar and to achieve the high $CO_2$ purities necessary for cost-effective sequestration.[12,13] While many different classes of adsorbents have been studied for $CO_2$ capture, the most promising materials have typically featured exposed metal cations, exposed anions, or alkylamines, all of which can have strong interactions with $CO_2$.[11] Despite the large number of adsorbents that have been reported in the context of $CO_2$ capture, the majority of studies have relied exclusively on pure $CO_2$ and $N_2$ isotherms, which has made it challenging to identify the best materials for capturing $CO_2$ from an actual flue gas mixture that has a significant amount of $H_2O$. This is particularly true for metal–organic frameworks and has hindered progress in the field.[14]

There have been some noteworthy computational and experimental efforts to evaluate the stability and $CO_2$ capture performance of metal–organic frameworks under more realistic conditions,[15,16] but to the best of our knowledge, there are no reports of multicomponent equilibrium adsorption isotherms for mixtures that include $CO_2$, $N_2$, and $H_2O$. In any gas separation application, mixed gas equilibrium adsorption data are critical for comparing the performances of different materials, for designing processes, and for validating theoretical models of mixture adsorption.[17] While models such as ideal adsorbed solution theory (IAST) can be used to predict adsorption for simple gas mixtures such as $CO_2$ and $N_2$ with reasonable confidence,[18,19] their accuracy is not well established for more complex mixtures such as $CO_2$, $N_2$, and $H_2O$.[20] More


DOI: 10.1021/jacs.5b00838
J. Am. Chem. Soc. 2015, 137, 4787–4803

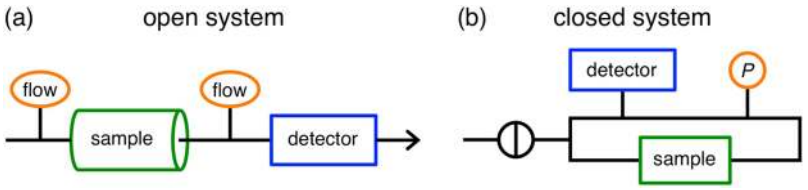


**Figure 2.** (a) In an open system multicomponent adsorption measurement, a mixture of gases is flowed over a packed bed of adsorbent. The flow rate and composition of the inlet and outlet gas streams are recorded until the composition of the outlet gas stream matches the inlet. (b) In a closed system multicomponent adsorption measurement, a mixture of gases is dosed to a sample and allowed to equilibrate. The amount of each component adsorbed is determined from the equilibrium gas-phase composition and either the equilibrium pressure in a volumetric measurement or the equilibrium weight in a gravimetric measurement.

importantly, all models that rely on single-component adsorption isotherms to predict mixed gas adsorption assume that the adsorbent is in the same thermodynamic state in the presence of each gas. For many adsorbents that exhibit structural or chemical changes specific to different gas molecules, this is most certainly not the case, and direct measurement of mixed gas adsorption is the only way to reliably evaluate gas separation performance.

In contrast to single-component adsorption measurements, which are now carried out routinely and with high accuracy using commercial instruments, mixed gas adsorption measurements are often time-consuming, requiring carefully designed custom equipment and complex data analysis.[21] As a result, there is a significant lack of mixed gas equilibrium adsorption data reported in the literature.[17] The limited mixed gas adsorption data available are mostly for two-component mixtures in zeolites, and equilibrium adsorption data for mixtures of more than two components are exceedingly rare, even though many industrial gas separations involve multicomponent mixtures.[17a,22]

More routinely, dynamic column breakthrough experiments are used to evaluate the separation performance of an adsorbent by flowing a mixture of gases through a packed bed and measuring the composition of the outlet gas stream as a function of time.[23] It is important to note that a typical breakthrough experiment does not yield equilibrium data, and the relationship between breakthrough results and equilibrium adsorption isotherms is not always clear.[17c] For instance, nearly all adsorbents will show at least some capacity for capturing $CO_2$ in a standard breakthrough experiment with a mixture of $CO_2$, $N_2$, and $H_2O$, since the front of the bed will desiccate the incoming gas mixture, leaving just $CO_2$ and $N_2$ as the gas flows through the bed.[24,25] This can lead to misleading conclusions about the intrinsic ability of a material to adsorb $CO_2$ at a specific partial pressure of $H_2O$, particularly when experiments are run on a small amount of sample. Indeed, many factors in addition to multicomponent adsorption capacities can influence experimental breakthrough curves, including column size, column shape, gas flow rates, adsorbent packing density, and extra-column effects.[26] Because breakthrough experiments mimic the dynamic conditions of a large-scale separation, they can be helpful in developing processes for $CO_2$ capture. However, multicomponent equilibrium experiments are better suited for comparing the properties of different materials under similar conditions, since the amount of each gas adsorbed is determined only by the partial pressure of each gas and the temperature. Moreover, these equilibrium data can be used to model any dynamic process using local equilibrium theory, where an equilibrium is assumed to exist between the gas and adsorbed phases at every cross-section of an adsorbent bed. While this assumption is never entirely true, it is a reasonable approximation for many processes and relies on accurate multicomponent equilibrium data.[27]

Here, we report the design and validation of a high-throughput instrument for the accurate measurement of multicomponent equilibrium adsorption at conditions relevant to post-combustion carbon capture. These measurements are used to compare the performance of 15 different metal−organic frameworks, activated carbons, zeolites, and amine-appended silicas that are representative of the wide range of adsorbents that have been studied for this application (Figure 1).

## RESULTS AND DISCUSSION

**Multicomponent Adsorption.** Although multicomponent adsorption experiments are far less common than single-component experiments in the literature, there has still been significant progress toward developing improved methods for mixed gas measurements. Since it is usually not possible to measure directly the composition of the adsorbed phase, the main challenge in any multicomponent experiment is determining the composition, or relative partial pressures, of the gas phase at equilibrium.[17,21] The composition of the adsorbed phase, as well as the amounts of each gas adsorbed, can then be calculated as the difference between the amount of each component added to the system and the amount that is still present in the gas phase at equilibrium. A variety of techniques have been developed for this purpose in both open and closed systems, but preforming measurements with high enough accuracy to provide meaningful results is not trivial and likely explains the lack of published multicomponent data. Often, the adsorption capacities determined from a multicomponent measurement have such high errors that it is impossible to compare the properties of different materials.[21] If done accurately, however, any open or closed system measurement should generate equivalent multicomponent adsorption data for a given set of equilibrium conditions. Methods for performing multicomponent measurements have been reviewed thoroughly in the literature,[17a,b,21,22] but will be briefly summarized here in the context of choosing an appropriate technique for high-throughput multicomponent adsorption measurements of $CO_2$, $N_2$, and $H_2O$ mixtures at conditions representative of a power plant flue gas.

In a typical open system experiment, a gas mixture is flowed over a packed bed of adsorbent until the composition of the outlet gas stream is the same as that of the inlet, with a mass spectrometer or gas chromatograph used to record the outlet gas composition (Figure 2a).[28] Determining the equilibrium amounts adsorbed of each gas requires the accurate measurement of both the inlet and outlet gas flow rates and compositions as well as appropriate corrections for extra-


DOI: 10.1021/jacs.5b00838
J. Am. Chem. Soc. 2015, 137, 4787−4803

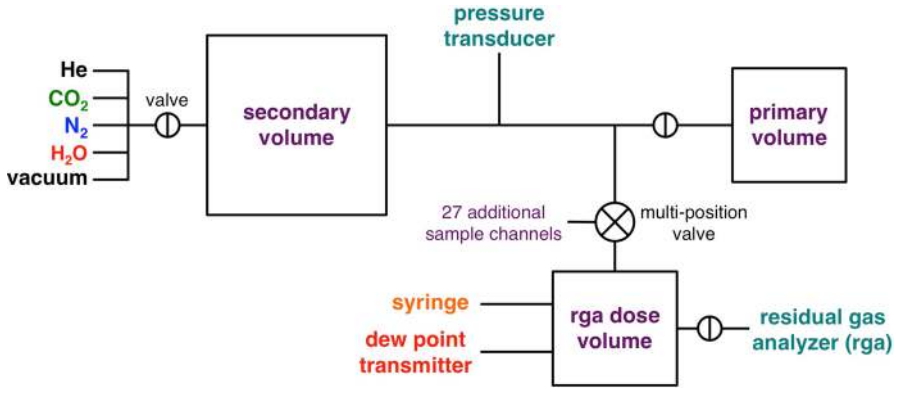


**Figure 3.** Simplified schematic of the high-throughput instrument used in this work to perform multicomponent adsorption measurements. Twenty-eight independent sample channels share a common gas-dosing manifold and are each connected to the residual gas analyzer (rga) dose volume via a multiposition valve. For multicomponent measurements, a mixture of gases is dosed into the secondary volume and rga dose volume, then expanded to the primary volume, which contains the activated adsorbent. The syringe is cycled multiple times, then the equilibrium pressure is recorded. For mixtures of $CO_2$, $N_2$, and $H_2O$, the dew point transmitter is used to record the partial pressure of $H_2O$, and the rga is used to measure the ratio of the partial pressures of $CO_2$ and $N_2$.

column effects and ensuring that the column is isothermal at equilibrium.[21] Because the equilibrium gas-phase composition is equivalent to the composition of the inlet gas stream, it is easy to compare the adsorption capacities of different materials under identical equilibrium conditions in an open system multicomponent experiment. Correcting for extra-column effects can, however, be extremely complicated. These corrections are critical to the accuracy of the results, particularly for small sample sizes where the dead volume of the system is not negligible.[26a] Additionally, it can be challenging to measure the outlet flow rate with high accuracy since the calibration of most flow meters is dependent on the composition of the gas that is flowing through them.[26b] As a result of these issues, open system measurements often require a large amount of sample in order to collect accurate data, and consequently are not very amenable to high-throughput screening.[21]

Closed system measurements, on the other hand, are typically more accurate, allowing multicomponent experiments to be performed on smaller quantities of sample.[21] Still, there are significant experimental challenges to using closed systems to measure multicomponent equilibrium adsorption in a high-throughput manner. In a typical closed system experiment, a mixture of gases is dosed to an evacuated sample from a calibrated dosing volume, and the gas-phase composition is recorded once the sample has reached equilibrium (Figure 2b).[29] Since equilibration times can often be on the order of hours or even days, a circulation pump, or other gas-mixing device that does not alter the amount of gas inside the closed system, is typically needed.[30] Similar to open system measurements, a mass spectrometer or gas chromatograph can be used to measure the composition of the gas phase after equilibrium is reached, but now care must be taken to ensure that the equilibrium conditions are not altered when the gas is analyzed.[21] The total amount adsorbed can be determined using standard volumetric or gravimetric techniques with calibrated volumes and a pressure transducer or with buoyancy corrections and a balance, respectively. Equilibrium amounts adsorbed can then be determined by material balance using the ideal gas law or an appropriate equation of state.

Unlike in open system measurements, it is often challenging to measure multicomponent adsorption consistently at a specific set of equilibrium conditions in a closed system since the composition of the dosed gas mixture required to achieve a specific gas-phase composition at equilibrium is difficult to predict.[21] In spite of this, closed systems are more amenable to automation and to comparing multicomponent adsorption for a large number of samples with high accuracy. More advanced versions of the open and closed multicomponent experiments described here have also been developed, including the zero length column technique,[31] total desorption analysis,[32] *in situ* infrared spectroscopy,[33] and the isotope exchange technique.[34] While each of these techniques has certain advantages and disadvantages, none are particularly well suited for high-throughput multicomponent measurements with mixtures of $CO_2$, $N_2$, and $H_2O$.

**High-Throughput Multicomponent Adsorption Instrument.** In this work, a closed system approach was used to develop a high-throughput adsorption instrument that can measure multicomponent adsorption for up to 28 samples at a time (Figure S13). The instrument, built by Wildcat Discovery Technologies Inc., has 28 independent sample channels that share a common gas-dosing manifold with inputs for up to 8 gases, including $H_2O$ (Figure 3). Each sample channel has a calibrated volume ("secondary volume") and a 1000 torr pressure transducer (MKS Seta Model 730 absolute capacitance manometer; accuracy = 0.25% reading), which are contained inside a heated enclosure that is maintained at 40 °C to minimize temperature fluctuation. Each secondary volume is connected via 1/16″ stainless steel tubing to a sample chamber ("primary volume"). The secondary volumes are each approximately 21 mL, while the primary volumes are each approximately 14 mL. The secondary volumes are also connected via 1/16″ stainless steel tubing to two Valco multiposition valves, with the 28 channels split evenly between the two valves. The multiposition valves allow each of the 28 channels to be independently opened to the shared 14 mL "rga dose volume" (rga = residual gas analyzer), which contains a mass spectrometer (MKS Microvision 2), a dew point transmitter (Vaisala, accuracy = ± 3 °C), and a 170 mL gastight syringe. All gas lines, dosing volumes, and sample volumes can be heated above 40 °C, allowing $H_2O$ dosing pressures of >70 mbar. Custom software allows multicomponent measurements to be performed in a fully automated manner with complete control over all test


DOI: 10.1021/jacs.5b00838
J. Am. Chem. Soc. 2015, 137, 4787−4803

parameters. To the best of our knowledge, this is the first instrument reported to be capable of performing high-throughput multicomponent adsorption measurements at equilibrium.

In order to accurately measure the sample mass, activated samples are loaded in tared 4 mL vials inside a glovebox under a $N_2$ atmosphere. The 4 mL vials are then inserted into aluminum sample assemblies that can each hold up to 7 vials and can be fully sealed while inside the glovebox, with a Schrader valve completing the seal above each sample. The sample assemblies are then transferred to the high-throughput adsorption instrument, and the headspace above each sample is fully evacuated. The instrument then actuates each Schrader valve, opening each sample channel to vacuum. Sample temperatures in the range of 25−150 °C are achieved using heating elements under the sample holders, and temperatures throughout the instrument are continuously recorded by eight thermocouples.

Pure-component adsorption isotherms up to a maximum pressure of 1.2 bar are measured using a standard volumetric technique. To ensure that all volume calibrations, pressure transducer calibrations, thermocouple readings, and adsorption calculations are accurate and that any leak rates are negligible, background adsorption isotherms were measured for empty sample holders on all 28 channels using He, $N_2$, $CO_2$, and $H_2O$ (Figure S14). The magnitude of the background adsorption was always found to be <5 $\mu$mol. For a typical sample size of 50 mg, this corresponds to a maximum error of <0.1 mmol/g.

All multicomponent measurements in this work were performed for mixtures of $CO_2$, $N_2$, and $H_2O$ at 25 or 40 °C. In a typical experiment, $H_2O$ was first dosed repeatedly to each sample. Since the 40 °C saturation pressure of $H_2O$ is just 73.8 mbar, several $H_2O$ doses were needed to ensure a reasonable partial pressure of $H_2O$ at equilibrium.[35] Once an adequate amount of $H_2O$ was added, a $CO_2$ and $N_2$ mixture of known composition was dosed to each sample. Although it is usually difficult to target specific equilibrium conditions in closed system multicomponent measurements, very similar equilibrium partial pressures could be achieved for each sample by selecting appropriate gas dosing pressures and compositions.

After all gases were dosed, the gastight syringe was cycled at least 15 times over several hours to force the free gas above the sample to mix, ensuring that the entire system was at equilibrium with a uniform gas-phase composition. At equilibrium, a pressure transducer was used to record the total pressure, and the dew point transmitter was used to record the partial pressure of $H_2O$ (Figure S15). Closing the valves between the secondary and primary volumes then isolated each sample, and the ratio of $CO_2$ to $N_2$ in the gas phase was determined by sampling from the secondary volume to the rga (Figures S16, S17). Since the rga operates under high vacuum and requires a low inlet pressure, the gas pressure must be lowered significantly prior to sampling. This was accomplished by expanding the gas into a series of large evacuated volumes in order to ensure that the gas-phase composition remained constant.

Before measuring any multicomponent data, empty sample holders were used to check the accuracy of the instrument by dosing known mixtures of $CO_2$, $N_2$, and $H_2O$, cycling the syringe, and using the pressure transducers, dew point transmitter, and rga to measure the partial pressures of $CO_2$, $N_2$, and $H_2O$ in the gas phase, just as would be done in a real multicomponent experiment. The calculated partial pressures were in very good agreement with the expected partial pressures over the full range of conditions targeted for the multicomponent experiments (Figure 4). A detailed error

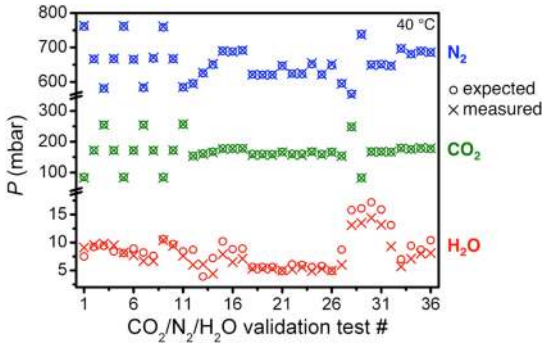


**Figure 4.** To validate the high-throughput multicomponent adsorption instrument, the experimentally measured partial pressures (crosses) of $N_2$ (blue), $CO_2$ (green), and $H_2O$ (red) are compared to the expected partial pressures (circles) of standard gas mixtures dosed into empty sample holders at 40 °C.

analysis can be found in the Supporting Information, but it is worth emphasizing that for just 50 mg of sample, the errors in the amounts of $CO_2$ and $N_2$ adsorbed are <0.2 mmol/g at a 95% confidence interval, and the error in the amount of $H_2O$ adsorbed is <0.3 mmol/g.

When drawing conclusions from multicomponent adsorption results, particularly with complex gas mixtures, it is always important to ensure that the system is truly at equilibrium when the amounts of each component adsorbed are determined.[17a] In order to ensure that the gastight syringe used in this work was cycled enough times to drive the complete system to an equilibrium, multicomponent measurements were performed for two metal−organic frameworks, mmen-$Mg_2$(dobpdc) (mmen = *N*,*N*′-dimethylethylenediamine, dobpdc$^{4-}$ = 4,4′-dioxido-3,3′-biphenyldicarboxylate) and mmen-$Ni_2$(dobpdc), with 0, 5, 10, 15, or 20 syringe cycles and with the samples being fully regenerated between each measurement. The multicomponent results are discussed in detail later, but it is important to note here that the measured amounts of $CO_2$, $N_2$, and $H_2O$ adsorbed did not vary within the error of the measurement once the syringe was cycled at least 5 times, demonstrating that the system had reached an equilibrium (Figure 5). As a result, we are confident that all multicomponent results presented in this work represent equilibrium amounts adsorbed, with the only exception being the amine-appended mesoporous silicas that exhibited exceedingly slow kinetics.

While single-component adsorption isotherms can be conveniently shown on two-dimensional plots since the amount adsorbed is only a function of total pressure, a complete description of the three-component adsorption isotherms measured here would require a four-dimensional plot since the amount adsorbed is a function of three partial pressures.[21] To simplify the presentation of the multicomponent results reported in this work, the amount of $CO_2$ adsorbed from a mixture of $CO_2$, $N_2$, and $H_2O$ is often plotted on the same two-dimensional plot as a single-component $CO_2$ adsorption isotherm. The single-component isotherm (green circles) effectively represents the amount of $CO_2$ that would be adsorbed at a given $CO_2$ partial pressure if $N_2$ and $H_2O$ had no effect, positive or negative, on $CO_2$ adsorption. The amount of


DOI: 10.1021/jacs.5b00838
J. Am. Chem. Soc. 2015, 137, 4787−4803

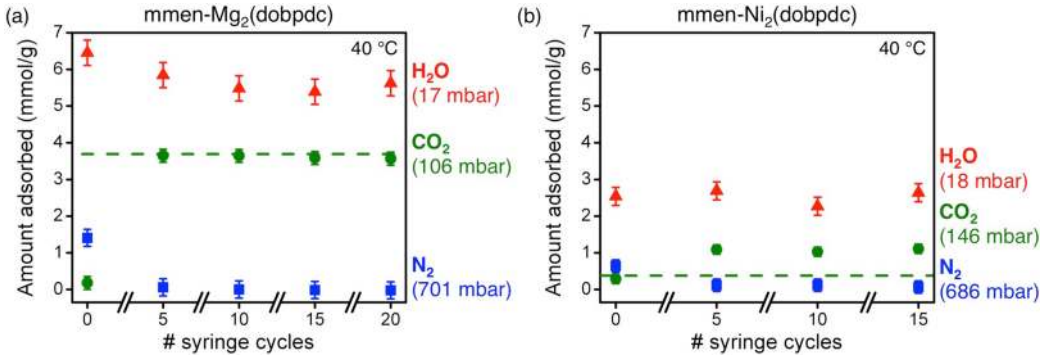


**Figure 5.** Amount of $CO_2$, $N_2$, and $H_2O$ adsorbed for (a) mmen-$Mg_2$(dobpdc) and (b) mmen-$Ni_2$(dobpdc) is plotted as a function of the number of times the gastight syringe was cycled to mix the headspace gas during a multicomponent experiment. For each multicomponent measurement, the samples were fully regenerated by heating to 100 °C under vacuum, and all experimental parameters were identical with the exception of the number of syringe cycles. The dashed green lines represent the amount of pure $CO_2$ adsorbed from a single-component isotherm at the same $CO_2$ partial pressure as the multicomponent experiment.

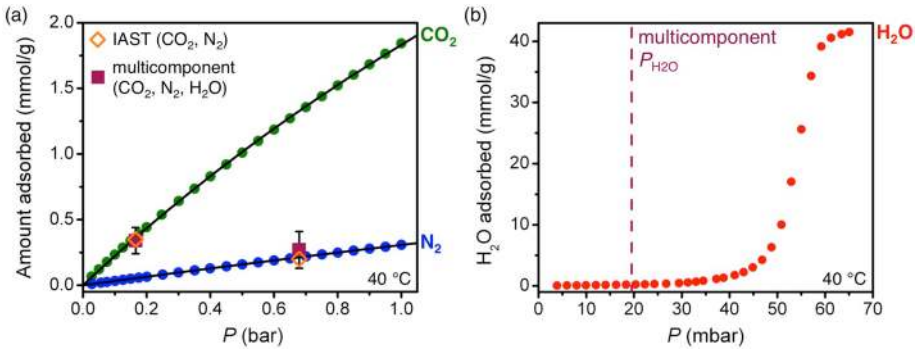


**Figure 6.** (a) Circles represent single-component $CO_2$ (green) and $N_2$ (blue) adsorption isotherms at 40 °C for the activated carbon AX-21. Black lines correspond to single-site Langmuir fits. Square data points represent the amount of $CO_2$ and $N_2$ adsorbed from a mixture of $CO_2$ (166 mbar), $N_2$ (679 mbar), and $H_2O$ (20 mbar) at 40 °C. Orange diamonds represent the amount of $CO_2$ and $N_2$ predicted to be adsorbed by IAST from a mixture of $CO_2$ (166 mbar) and $N_2$ (679 mbar). (b) Pure $H_2O$ adsorption isotherm (red circles) for AX-21 at 40 °C. The purple dashed line represents the partial pressure of $H_2O$ in the multicomponent experiment.

$CO_2$ adsorbed from a mixture of $CO_2$, $N_2$, and $H_2O$ is then plotted using a square symbol at the appropriate partial pressure of $CO_2$, and this value can be easily compared to the pure $CO_2$ isotherm to gauge the effect of $N_2$ and $H_2O$ on $CO_2$ adsorption. The partial pressure of $H_2O$ is indicated by the color of the square data points, with the partial pressure of $H_2O$ increasing from blue to purple to red. For nearly all multicomponent experiments reported here, the equilibrium partial pressure of $N_2$ is very close to 700 mbar. All error bars shown correspond to ±1.96 standard deviations (95% confidence interval).

Note that these two-dimensional plots do not include any information about the amount of $N_2$ or $H_2O$ adsorbed at equilibrium, but these values are included in the Supporting Information. For carbon capture applications, the amount of $N_2$ adsorbed is needed to determine the purity of captured $CO_2$, while the amount of $H_2O$ adsorbed is important for evaluating the energy required to regenerate the adsorbent and to compress the $CO_2$. Except for a few cases discussed below, the multicomponent $N_2$ adsorption capacities at equilibrium are within error of zero. Before considering $N_2$ and $H_2O$ adsorption, however, an adsorbent must at least maintain some capacity for $CO_2$ in the presence of $N_2$ and $H_2O$ in order to have any use in $CO_2$ capture. In the following sections, the multicomponent instrument is used to directly measure the amount of $CO_2$ adsorbed at flue gas-like conditions for adsorbents with surface chemistries and binding sites representative of the most studied materials for $CO_2$ capture, including those featuring nonpolar surfaces, exposed metal cations, exposed anions, and alkylamines.

**Nonpolar Surfaces.** Many high surface area metal−organic frameworks and activated carbons have relatively nonpolar pore surfaces that lack any strong $CO_2$ binding sites, resulting in materials with little affinity for $CO_2$ at low pressures. For instance, $Zn_4O(bdc)_3$ ($bdc^{2-}$ = 1,4-benzenedicarboxylate; MOF-5)[36] and the activated carbon AX-21 (Maxsorb)[37] have Langmuir surface areas of 3995 and 4880 $m^2/g$ but adsorb only 0.1 mmol/g (0.4 wt %) and 0.3 mmol/g (1.3 wt %) of $CO_2$ at 0.15 bar and 40 °C, respectively. Although many adsorbents have significantly higher 0.15 bar $CO_2$ capacities, most materials with nonpolar surfaces are relatively hydrophobic, and as a result, they have attracted some interest for post-combustion carbon capture.[11a,38,39]

As is the case for many activated carbons, AX-21 has a classical type V $H_2O$ isotherm at 40 °C; there is negligible $H_2O$ adsorption on its hydrophobic pore surface until pressures above 45 mbar, at which point clustering of $H_2O$ molecules on the surface leads to a sharp increase in the amount of $H_2O$ adsorbed (Figure 6b).[40,41] As long as the partial pressure of $H_2O$ is kept below 45 mbar ($p/p_0$ = 0.61), $H_2O$ adsorption should be negligible and would not be expected to interfere with $CO_2$ adsorption. To confirm this, a multicomponent


DOI: 10.1021/jacs.5b00838
J. Am. Chem. Soc. 2015, 137, 4787−4803

Table 2. Physical Properties of $CO_2$, $N_2$, and $H_2O$[17a]

| | $CO_2$ | $N_2$ | $H_2O$ |
|---|---|---|---|
| kinetic diameter (Å) | 3.3−3.9 | 3.64−3.80 | 2.64 |
| polarizability ($\times 10^{-25}$ cm$^3$) | 26.5 | 17.6 | 14.5 |
| dipole moment ($\times 10^{18}$ esu·cm) | 0 | 0 | 1.87 |
| quadrupole moment ($\times 10^{-26}$ esu·cm$^2$) | 4.30 | 1.52 | – |

adsorption experiment was performed for a mixture of $CO_2$, $N_2$, and $H_2O$ in AX-21 at 40 °C and equilibrium partial pressures of 166, 679, and 20 mbar, respectively (Figure 6a). As expected, no $H_2O$ is adsorbed under these conditions, and the amount of $CO_2$ adsorbed is 0.3(1) mmol/g, within error of the amount adsorbed from pure $CO_2$ at the same pressure. Moreover, the experimental amounts of $CO_2$ and $N_2$ adsorbed in the presence of $H_2O$ match IAST predictions for a binary mixture of just $CO_2$ and $N_2$.

While AX-21 has some capacity for $CO_2$ and negligible $H_2O$ adsorption under these conditions, it has very poor $CO_2/N_2$ selectivity with nearly the same amount of $N_2$ adsorbed as $CO_2$. It is also important to note that the partial pressure of $H_2O$ in 40 °C flue gas is nearly 70 mbar, so the flue gas would likely need to be dried to below 45 mbar for $H_2O$ adsorption to remain negligible. There may, however, be other adsorbents with type V $H_2O$ isotherms at 40 °C that have a step closer to 70 mbar. Regardless, materials with higher selectivities for $CO_2$ over $N_2$ and higher $CO_2$ capacities at 0.15 bar will require stronger adsorption sites than are likely to be found in adsorbents with entirely nonpolar surfaces. Since minimizing $H_2O$ adsorption is important to lowering the regeneration energy in a carbon capture process, designing adsorbents that have both hydrophobic surfaces and strong $CO_2$ binding sites is a key challenge in developing a next generation of carbon capture materials.

**Exposed Metal Cations.** Owing to its larger quadrupole moment and greater polarizability (Table 2), $CO_2$ will have a stronger electrostatic interaction than $N_2$ with an exposed partial charge. By incorporating metal cations with open coordination sites into metal−organic frameworks and zeolites, exposed positive charges can be created that act as strong $CO_2$ adsorption sites,[42,43] leading to materials with some of the highest reported 0.15-bar capacities for $CO_2$ and selectivities for $CO_2$ over $N_2$. In many zeolites, exposed positive charges result from extra-framework cations that are present in the pores to balance the negative charge generated from replacing a fraction of the $Si^{4+}$ cations in pure silica zeolites with $Al^{3+}$. Zeolite 13X ($NaAlSi_{1.18}O_{4.36}$; FAU, Na-X) and zeolite 5A ($Na_{0.28}Ca_{0.36}AlSiO_4$; LTA, Ca-A), for instance, feature extra-framework $Na^+$ and/or $Ca^{2+}$ cations that strongly adsorb $CO_2$.[44] For certain metal−organic frameworks, exposed metal cations can be generated directly on the framework by post-synthetically removing metal-bound solvent molecules. Exposed $Mg^{2+}$, $Ni^{2+}$, $Cu^{2+}$, and $Fe^{3+}$ cations of this type are present in $Mg_2$(dobdc) (dobdc$^{4-}$ = 2,5-dioxido-1,4-benzenedicarboxylate; Mg-MOF-74, CPO-27-Mg),[43,45] $Ni_2$(dobdc) (Ni-MOF-74, CPO-27-Ni),[46] $Cu_3(btc)_2$ (btc$^{3-}$ = 1,3,5-benzenetricarboxylate; HKUST-1),[47] and $Fe_3OX(btc)_2$ (X = OH, F; Fe-MIL-100),[48] respectively.

**Zeolites 5A, 13X, and $M_2$(dobdc).** Zeolite 5A adopts the LTA (Linde Type A) structure type, wherein sodalite cages are connected via square faces to form a three-dimensional cubic framework of 4.2 Å diameter pores. Extra-framework $Na^+$ and $Ca^{2+}$ cations are located at the six-ring windows ($Si_nAl_{6-n}O_6$) of the sodalite cages.[49] Zeolite 13X adopts the FAU (faujasite) structure type, wherein sodalite cages are connected via hexagonal faces to form a three-dimensional cubic framework of 7.4 Å diameter pores. Extra-framework $Na^+$ cations are located primarily above the plane of the four-ring and six-ring windows of the sodalite cages.[50] In contrast to zeolites 5A and 13X, the exposed metal cations in the metal−organic frameworks $Mg_2$(dobdc) and $Ni_2$(dobdc) are part of the framework structure, in which helical chains of square pyramidal $Mg^{2+}$ or $Ni^{2+}$ cations, respectively, are bridged by dobdc$^{4-}$ ligands to form 12 Å hexagonal channels (Figure 1).

Because of their high density of exposed metal cations, $Mg_2$(dobdc), $Ni_2$(dobdc), zeolite 13X, and zeolite 5A each adsorb over 3.1 mmol/g (12 wt %) of $CO_2$ at 0.15 bar and 40 °C and have been extensively studied for carbon capture applications (Figure 7).[12a,b,16a,c−e,43,44,51] In fact, the 5.3

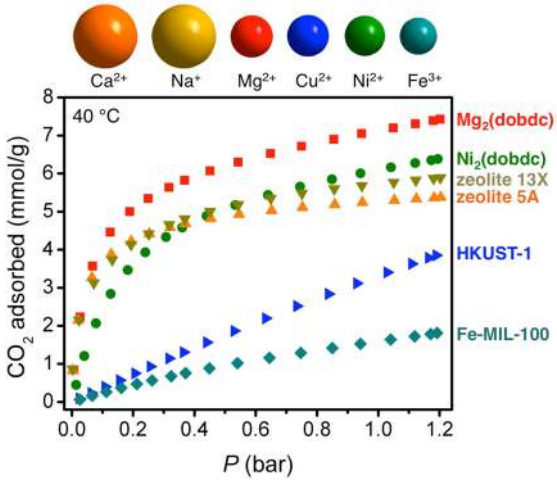


**Figure 7.** Pure $CO_2$ adsorption isotherms at 40 °C for metal−organic frameworks and zeolites that feature exposed $Ca^{2+}$, $Na^+$, $Mg^{2+}$, $Cu^{2+}$, $Ni^{2+}$, or $Fe^{3+}$ cations.

mmol/g (18.9 wt %) of $CO_2$ adsorbed by $Mg_2$(dobdc) at 0.15 bar and 40 °C is the highest uptake reported for any solid adsorbent under these conditions.[11d] While the majority of studies on the carbon capture potential of metal−organic frameworks and zeolites with exposed metal cations have relied exclusively on single-component $CO_2$ and $N_2$ adsorption isotherms, there has been some work toward understanding the effect of $H_2O$ on $CO_2$ capacity and selectivity.

Not surprisingly, DFT calculations have shown that $H_2O$, with its strong dipole moment, is expected to have a much greater affinity than $CO_2$ for exposed metal cation adsorption sites.[52] Several experimental studies have used binary adsorption measurements for mixtures of $CO_2$ and $H_2O$ in zeolites 13X and 5A to show that $CO_2$ adsorption is indeed significantly reduced at low partial pressures of $H_2O$.[53] While initial breakthrough studies suggested that $H_2O$ did not adversely affect the adsorption properties of $Mg_2$(dobdc),[51a]


DOI: 10.1021/jacs.5b00838
J. Am. Chem. Soc. 2015, 137, 4787−4803

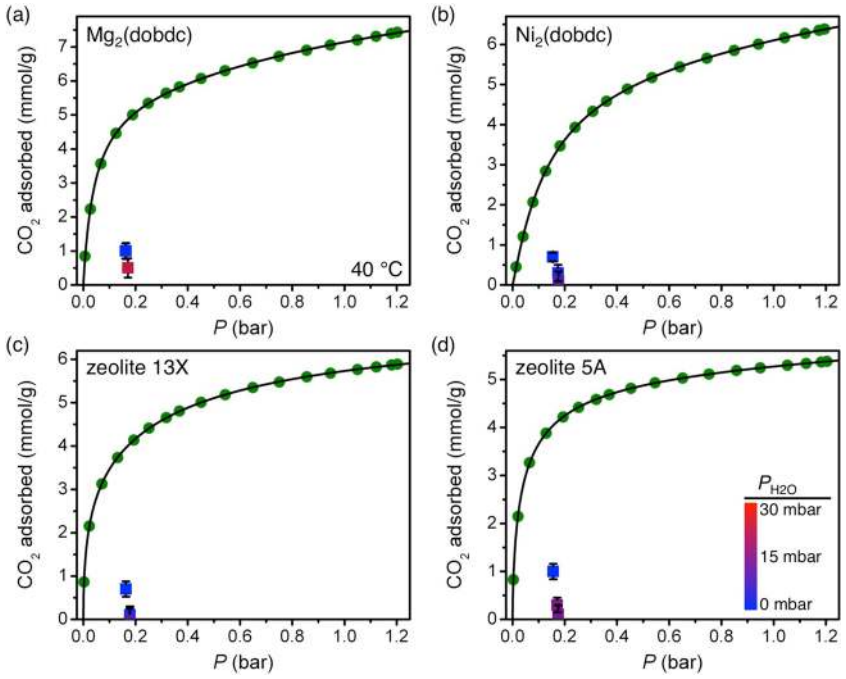


**Figure 8.** A summary of multicomponent equilibrium measurements at 40 °C for (a) $Mg_2$(dobdc), (b) $Ni_2$(dobdc), (c) zeolite 13X, and (d) zeolite 5A. Green circles represent pure $CO_2$ adsorption isotherms for each compound, and black lines are the corresponding single- or dual-site Langmuir fits. Square data points represent the amount of $CO_2$ adsorbed from a mixture of $CO_2$, $N_2$, and $H_2O$, and the color of the square indicates the equilibrium partial pressure of $H_2O$, with the partial pressure of $H_2O$ increasing from blue to purple to red. The exact values of $P_{H_2O}$ can be found in Table S3. For all multicomponent data points, the partial pressure of $N_2$ is 680−700 mbar.

this was eventually challenged by two experimental studies that showed a significant decrease in the pure $CO_2$ adsorption of $Mg_2$(dobdc) and $Ni_2$(dobdc) after exposure to mixtures containing $CO_2$ and $H_2O$.[16d,e] Additionally, the amount of $CO_2$ adsorbed at 25 °C was measured for $Ni_2$(dobdc) at different $H_2O$ loadings, revealing a continuous decrease in $CO_2$ adsorption with increasing $H_2O$ loading.[16c]

Under dynamic breakthrough conditions, a recent study found that $Ni_2$(dobdc) retained a $CO_2$ capacity of 2.2 mmol/g (8.8 wt %) in the presence of a 15:85 mixture of $CO_2$:$N_2$ with 3% RH (0.95 mbar $H_2O$) at 25 °C and a total pressure of 1 bar.[54] Based on these results, it was suggested that $Ni_2$(dobdc) could be used for $CO_2$ capture from flue gas, provided a desiccant was used to pre-dry the gas to around 1 mbar of $H_2O$. We note, however, that this measurement was not performed under equilibrium conditions, and that the average partial pressure of $H_2O$ in the bed at the time of $CO_2$ breakthrough was likely significantly below 1 mbar. Since the column was only cycled three times, these experiments may not adequately capture the expected buildup of bound $H_2O$ over time, particularly if the $H_2O$ adsorption front remained close to the column inlet in each experiment.[25] Moreover, the $CO_2$ breakthrough capacity will be highly dependent on the exact set of dynamic conditions used, and the results may not necessarily translate to larger scales. As an alternative, multicomponent experiments can be used to directly evaluate the effects of different partial pressures of $H_2O$ on $CO_2$ capacity at equilibrium conditions similar to those expected in an actual $CO_2$ capture process.

In this work, three-component adsorption measurements were performed with mixtures of $CO_2$, $N_2$, and $H_2O$ at 40 °C for $Mg_2$(dobdc), $Ni_2$(dobdc), zeolite 13X, and zeolite 5A, and all results clearly show a significant decrease in the amount of $CO_2$ adsorbed in the presence of $N_2$ and $H_2O$ (Figure 8). In fact, the amount of $CO_2$ adsorbed in all four materials decreases to <25% of the pure-component value at $H_2O$ partial pressures of <2 mbar. The multicomponent results for zeolites 13X and 5A are in excellent agreement with previously reported binary adsorption equilibria for mixtures of $CO_2$ and $H_2O$ at similar conditions.[53b] The multicomponent result for $Ni_2$(dobdc), however, differs significantly from the amount of $CO_2$ adsorbed in the previously reported breakthrough experiment, where a substantial $CO_2$ capacity was still observed at a low partial pressure of $H_2O$.[54] These conflicting results can be attributed to the fact that the breakthrough experiment was performed under dynamic conditions with the adsorbent exposed to a range of $H_2O$ partial pressures below 1 mbar, while the multicomponent experiment was at equilibrium.

At even higher $H_2O$ partial pressures of 10−25 mbar, which are still well short of the >70 mbar expected in a flue gas, all four of these materials have high $H_2O$ adsorption and a negligible $CO_2$ capacity, directly confirming that $H_2O$ fully outcompetes $CO_2$ for the exposed metal cations under equilibrium carbon capture conditions (Figure 8). In order for any of these materials to be used in a carbon capture process, the flue gas would need to be dried significantly. While part of the adsorbent bed could be sacrificed to dry the incoming flue gas rather than capture $CO_2$,[24] this would almost certainly be more expensive than processes based on materials that can selectively capture $CO_2$ in the presence of high partial pressures of $H_2O$.

On a more fundamental level, it is worth mentioning that pervious *in situ* diffraction studies of $CO_2$ adsorption in zeolite 5A found that, in addition to exposed $Na^+$ and $Ca^{2+}$ cations, $CO_2$ is also strongly adsorbed at the center of eight-ring windows ($Si_nAl_{8-n}O_8$) because of several close interactions


DOI: 10.1021/jacs.5b00838
J. Am. Chem. Soc. 2015, 137, 4787−4803

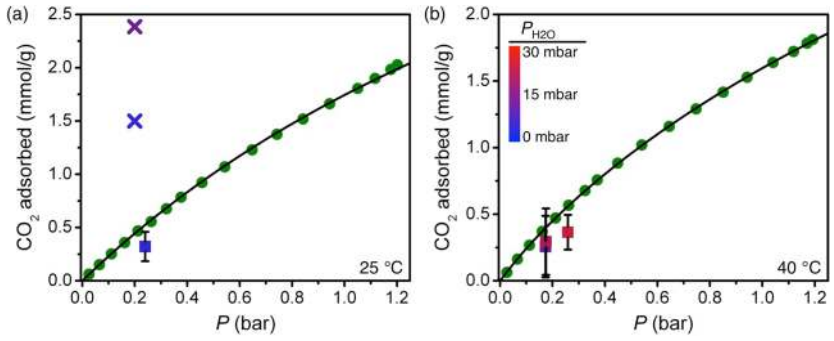


**Figure 9.** A summary of $CO_2$, $N_2$, $H_2O$ multicomponent equilibrium measurements for Fe-MIL-100 at (a) 25 °C and (b) 40 °C. Green circles represent pure $CO_2$ adsorption isotherms at each temperature, and black lines are the corresponding dual-site Langmuir fits. Square data points represent the amount of $CO_2$ adsorbed from a mixture of $CO_2$, $N_2$, and $H_2O$, and the color of the square indicates the equilibrium partial pressure of $H_2O$. The exact values of $P_{H_2O}$ can be found in Table S3. Crosses represent the amount of $CO_2$ adsorbed at 25 °C and 6.3 mbar of $H_2O$ (blue) or 12.7 mbar of $H_2O$ (purple), as determined from previous breakthrough experiments.[58]

between $CO_2$ and zeolite O atoms.[44c] It had been suggested that these eight-ring sites, which were also shown to strongly adsorb $CO_2$ in the Chabazite-type zeolite Cu-SSZ-13, may still be able to bind $CO_2$ in the presence of $H_2O$,[55] but the multicomponent results do not support this. Additional diffraction studies are needed to probe whether the lack of $CO_2$ adsorption in the presence of $H_2O$ is due to $H_2O$ binding directly to the eight-ring sites preferentially over $CO_2$ or due to $H_2O$ adsorption at the exposed metal cations blocking access of $CO_2$ to the eight-ring sites.

**HKUST-1.** The metal−organic framework HKUST-1 is composed of $Cu_2$-paddlewheel units bridged by 1,3,5-benzenetricarboxylate to form a cubic structure with three types of microporous cages (Figure 1).[47] Although the exposed $Cu^{2+}$ cations in HKUST-1 have a weaker interaction with $CO_2$ than the exposed $Na^+$ and $Ca^{2+}$ cations of zeolites 13X and 5A or the exposed $Mg^{2+}$ and $Ni^{2+}$ cations of $M_2$(dobdc),[56] with just 0.6 mmol/g (2.6 wt %) of $CO_2$ adsorbed at 0.15 bar and 40 °C, previous experimental and theoretical studies found an increase in the amount of $CO_2$ adsorbed at low loadings of $H_2O$.[16b] More specifically, the amount of $CO_2$ adsorbed at 25 °C was shown to increase by roughly 160%, from 2.2 mmol/g (8.8 wt %) at 0.29 bar to 3.6 mmol/g (13.7 wt %) at 0.24 bar when 2.3 mmol/g of $H_2O$ was pre-adsorbed (0.46 $H_2O$ molecules per $Cu^{2+}$ site). This increase was attributed to a stronger electrostatic interaction between Cu-bound $H_2O$ and $CO_2$ than between exposed $Cu^{2+}$cations and $CO_2$.[16b] A later study on a pelletized sample of HKUST-1 also found an increase in $CO_2$ adsorption at low $H_2O$ loadings, albeit to a much smaller extent.[16c]

In this work, multicomponent measurements were used to measure the $CO_2$ capacity of HKUST-1 at conditions more representative of a post-combustion flue gas (Figure S8). Interestingly, we do not observe a significant change in the amount of $CO_2$ adsorbed by HKUST-1 at 40 °C with 1.9(3) mmol/g of $H_2O$ adsorbed (0.38 $H_2O$ per $Cu^{2+}$; $P_{H_2O}$ = 0.001 bar) and $CO_2$ and $N_2$ partial pressures of 0.161 and 0.686 bar, respectively. Because of the error in the multicomponent $CO_2$ adsorption uptake, it is not possible to distinguish between a moderate increase in $CO_2$ adsorption of up to 0.3 mmol/g and a slight decrease of up to 0.1 mmol/g from the pure-component capacity of 0.6 mmol/g based on this single measurement. Somewhat unexpectedly, we still observe the same amount of $CO_2$ adsorbed at an even higher equilibrium $H_2O$ loading of 7.7 mmol/g (1.54 $H_2O$ per $Cu^{2+}$; $P_{H_2O}$ = 0.004 bar), which is well past the point at which all $Cu^{2+}$ sites should be saturated with $H_2O$. This could be explained by the fact that two strong $CO_2$ adsorption sites exist in HKUST-1: at the exposed $Cu^{2+}$ cations (5.0 mmol/g) and at the center of the windows of the small octahedral cages (3.3 mmol/g).[51c] It is possible that $CO_2$ has a strong interaction with Cu-bound $H_2O$ as was previously suggested; however, it seems more likely that, provided the $CO_2$ binding energy at each site is similar, the constant $CO_2$ capacity at $H_2O$ loadings below 8 mmol/g is due to $CO_2$ adsorption still occurring at the window sites even as $H_2O$ begins to block the exposed $Cu^{2+}$ cations. Regardless, at higher $H_2O$ partial pressures closer to the 0.075 bar expected in flue gas, all strong $CO_2$ binding sites are likely occupied or blocked by adsorbed $H_2O$ molecules, and HKUST-1 has a negligible $CO_2$ capacity. This result is in agreement with previous binary measurements performed at 25 °C.[16c,25]

**Fe-MIL-100.** The metal−organic framework Fe-MIL-100 is composed of $\mu_3$-O-centered trinuclear iron(III) clusters that are bridged by 1,3,5-benzenetricarboxylate to form a three-dimensional network of supertetrahedra, wherein microporous windows provide entrances to mesoporous cages (Figure 1).[48] While one-third of the $Fe^{3+}$ cations are ligated by a charge-balancing $OH^-$ or $F^-$ anion, bound solvent can be removed from the remaining $Fe^{3+}$ centers during activation to give five-coordinate exposed metal cations.[57] Intriguingly, it was reported that the amount of $CO_2$ adsorbed at 25 °C from a mixture of $CO_2$, $N_2$, and $H_2O$ at 20% RH (6.3 mbar $H_2O$) or 40% RH (12.7 mbar $H_2O$) increased 3-fold or 5-fold, respectively, from the pure $CO_2$ capacity.[58] This dramatic increase in $CO_2$ uptake was determined from a breakthrough-type experiment after pre-equilibrating Fe-MIL-100 with $H_2O$ vapor and was tentatively attributed to the formation of microporous pockets created by partial $H_2O$ filling of the mesoporous cages. Even more surprisingly, the $CO_2$ adsorption enthalpy at 40% RH was determined using microcalorimetry to be just −1 kJ/mol, which was believed to be the result of endothermic $H_2O$ desorption offsetting exothermic $CO_2$ adsorption.

Because of the significance of these results, we attempted to reproduce this increase in $CO_2$ adsorption under equilibrium conditions. After synthesizing Fe-MIL-100 and confirming that the surface area and 25 °C $CO_2$ adsorption isotherm matched those previously reported (Figures S7, S9), multicomponent measurements were performed at both 25 and 40 °C and at


DOI: 10.1021/jacs.5b00838
J. Am. Chem. Soc. 2015, 137, 4787−4803

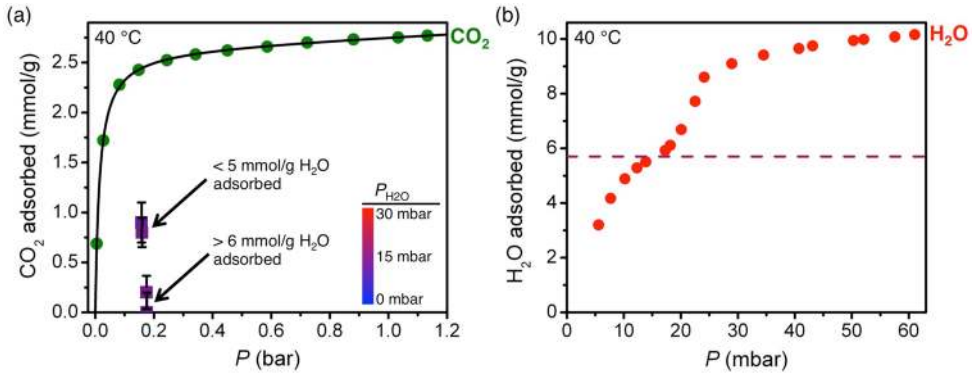


**Figure 10.** (a) A summary of $CO_2$, $N_2$, $H_2O$ multicomponent equilibrium measurements for $Zn(pyz)_2(SiF_6)$ at 40 °C. Green circles represent a pure $CO_2$ adsorption isotherm, and the black line is the corresponding dual-site Langmuir fit. Square data points represent the amount of $CO_2$ adsorbed from a mixture of $CO_2$, $N_2$, and $H_2O$, and the color of the square indicates the equilibrium partial pressure of $H_2O$. The exact values of $P_{H_2O}$ can be found in Table S3. (b) Pure $H_2O$ adsorption isotherm (red circles) for $Zn(pyz)_2(SiF_6)$ at 40 °C.

different partial pressures of $H_2O$. Regardless of whether the measurement was at 25 or 40 °C, we consistently observe a slight decrease in the amount of $CO_2$ adsorbed in the presence of $N_2$ and $H_2O$, even at equilibrium partial pressures that are nearly identical to the previously reported breakthrough conditions (Figure 9). Note that the crosses in the 25 °C multicomponent plot of Figure 9 represent the previously reported $CO_2$ breakthrough capacities.[58] Further work is necessary to determine the origin of these conflicting results and to establish why a 5-fold increase in $CO_2$ adsorption might be observed under dynamic conditions, but not at equilibrium.

**Exposed Anions.** Exposed negative charges are much less common in metal−organic frameworks than exposed positive charges, but just as a positive charge can attract the electronegative O atoms of $CO_2$, a negative charge can attract its electropositive C atom.[59] The compound $Zn(pyz)_2(SiF_6)$ provides an important example of a three-dimensional framework with exposed anions. Its structure is composed of square grids of $Zn^{2+}$ and pyrazine pillared by hexafluorosilicate ($SiF_6^{2-}$) anions to form one-dimensional channels that have a 3.8 Å diagonal dimension (Figure 1).[60] Although the octahedral Zn cations are coordinatively saturated, the combination of small pores and exposed $F^-$ anions that protrude from the corners of each channel leads to strong $CO_2$ adsorption at low pressures, with a low-coverage heat of adsorption of −45 kJ/mol and a capacity of 2.4 mmol/g (9.6 wt %) at 40 °C and 0.15 bar. Even more significantly, breakthrough experiments performed for a mixture of 10% $CO_2$ in $N_2$ at 74% RH (23.5 mbar $H_2O$) at 25 °C suggested that $H_2O$ has a negligible effect on the ability of the material to adsorb $CO_2$ selectively at high capacity.[59a]

In this work, multicomponent experiments were used to compare the equilibrium capacity and selectivity of $Zn(pyz)_2(SiF)_6$ for $CO_2$ in the presence of $N_2$ and $H_2O$ to the earlier breakthrough results. Toward this end, a sample of $Zn(pyz)_2(SiF_6)$ was synthesized, and the resulting $CO_2$ adsorption isotherms were found to be in close agreement to those previously reported (Figure S11). While previously reported variable temperature powder X-ray diffraction experiments indicated that $Zn(pyz)_2(SiF_6)$ was stable to 250 °C under vacuum,[59a] our thermogravimetric analysis results show rapid thermal decomposition occurring above 115 °C (Figure S12), which is in agreement with the initial report on the thermal stability of $Zn(pyz)_2(SiF_6)$.[60] The reasons for these differences are not clear, but this low thermal stability could be problematic for designing a temperature swing adsorption process with a reasonable $CO_2$ working capacity.[12b] Regardless, the multicomponent measurements performed here show that at 40 °C and an $H_2O$ equilibrium partial pressure of 13 mbar, the amount of $CO_2$ adsorbed at a partial pressure of 0.16 bar decreased by 60% to 0.9(2) mmol/g, and the amount of $N_2$ adsorbed at a partial pressure of 0.7 bar was within error of 0 mmol/g (Figure 10a). Under these equilibrium conditions, it thus appears that $Zn(pyz)_2(SiF_6)$ retains at least some capacity for $CO_2$ and a high selectivity over $N_2$, but $H_2O$ is clearly affecting the $CO_2$ capture properties in contrast to the previously reported dynamic breakthrough results.

Surprisingly, when repeating this multicomponent measurement on a fresh sample, we found that the amount of $CO_2$ adsorbed at nearly identical equilibrium partial pressures had dropped to within error of 0 mmol/g (Figure 10a). While the partial pressure of $H_2O$ was 13 mbar in both measurements, the amount of $H_2O$ adsorbed had increased from 3.8(3) to 6.4(4) mmol/g. Such significant changes in the amount of $CO_2$ and $H_2O$ adsorbed at nearly constant partial pressures are indicative of a phase transition, something that was previously suggested to occur based on X-ray powder diffraction experiments at increasing partial pressures of $H_2O$.[59a] To investigate this further, a pure-component $H_2O$ isotherm was measured at 40 °C and found to have an inflection at an $H_2O$ loading of nearly 6 mmol/g (Figure 10b). The multicomponent results and pure-component $H_2O$ isotherm are thus consistent with a phase change occurring at $H_2O$ loadings above 6 mmol/g and leading to an unknown material with no capacity or selectivity for $CO_2$ adsorption in the presence of $H_2O$. Since this phase change would occur at the over 70 mbar of $H_2O$ that is present in flue gas, it seems unlikely that $Zn(pyz)_2(SiF_6)$ could be used in a post-combustion carbon capture process without significant drying of the flue gas, even if the phase change is fully reversible.

Still, it is interesting that $Zn(pyz)_2(SiF_6)$ has a reasonable capacity for $CO_2$ and a high selectivity over $N_2$ before the phase change occurs, and it would be useful to determine exactly where $CO_2$ and $H_2O$ adsorb in the framework under these conditions. Moreover, it would be informative to measure a similar compound with exposed anions that does not exhibit a phase change to determine the amount of $CO_2$ adsorbed, if any, at higher partial pressures of $H_2O$. Additionally, the reasons for


DOI: 10.1021/jacs.5b00838
J. Am. Chem. Soc. 2015, 137, 4787−4803

the very different $CO_2$ capacities observed for $Zn(pyz)_2(SiF_6)$ under dynamic breakthrough and equilibrium conditions are not clear and need to be understood. We note, however, that the $CO_2$ breakthrough capacity appears to have been determined simply by multiplying the $CO_2$ breakthrough time by the $CO_2$ flow rate at the inlet of the column, and it is unclear how much $H_2O$ was in the column at the breakthrough time and whether or not any extra-column effects were taken into account.[59a]

**Alkylamines.** Owing to their ability to capture high-purity $CO_2$ in the presence of $N_2$ and $H_2O$, aqueous amine solutions have been the most studied carbon capture technology to date.[10] However, amine solutions suffer from several drawbacks that have prevented major reductions in the cost of captured $CO_2$, despite nearly 40 years of research and optimization.[5] Most importantly, the concentration of amines in water is limited to 30−40 wt % to minimize corrosion and degradation issues,[61] which in turn limits the $CO_2$ capacity of the solutions and leads to high regeneration energies, as a significant amount of heat is wasted boiling water rather than desorbing $CO_2$. Incorporating amines into solid adsorbents represents a promising strategy for increasing $CO_2$ capacity and reducing regeneration energy while maintaining a high selectivity for $CO_2$ over other flue gas components.[11a]

In designing amine-based adsorbents, it is important to consider that isolated amine groups do not have a particularly strong affinity for $CO_2$. Rather, strong $CO_2$ binding only occurs when the amine binding $CO_2$ can transfer a proton to another Lewis base. Typically, this proton transfer occurs to another amine to form an ammonium carbamate, resulting in an overall amine:$CO_2$ stoichiometry of 2:1 (Scheme 1).[62] In humid gas

**Scheme 1. Under Dry Conditions, Reaction of $CO_2$ with 2 equiv of a 1° or 2° Alkylamine Amine Typically Forms Ammonium Carbamate**

mixtures, $H_2O$ can participate in the reaction of $CO_2$ with an amine, often leading to the formation of ammonium bicarbonate and an overall amine:$CO_2$ stoichiometry of 1:1 (Scheme 2).[63]

**Scheme 2. Under Humid Conditions, Reaction of $CO_2$ with 1 equiv of a 1° or 2° Alkylamine Typically Forms Ammonium Bicarbonate**

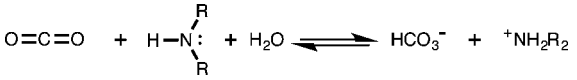

**Amine-Functionalized Mesoporous Silicas.** Early efforts to incorporate amines into porous materials focused primarily on mesoporous silicas. With BET surface areas ranging from 500 to 1500 $m^2/g$, a high density of amines can be impregnated inside or grafted directly onto the pore surface of a mesoporous silica.[64] While there has been some controversy as to the exact nature of adsorbed $CO_2$ inside these materials, it is now generally accepted that $CO_2$ reacts to form an ammonium carbamate under dry conditions (0.5 $CO_2$ per amine) and ammonium bicarbonate (1 $CO_2$ per amine) under humid conditions, provided that the silica has a high density of 1° or 2° amines.[62b,65] It is important to note that although these are the thermodynamically favored products under each set of conditions, ammonium carbamate formation occurs at a much faster rate than bicarbonate formation.[66] As a result, it can take a very long time to reach a full equilibrium capacity of 1 $CO_2$ per amine in the presence of $H_2O$, as there is often a mixture of ammonium carbamate and bicarbonate present before equilibrium is reached. This perhaps explains the wide range of $CO_2$ to amine ratios that have been reported for different amine-appended or -impregnated silicas in the presence of $H_2O$.[11a] Additionally, the majority of reports on the equilibrium $CO_2$ capacity of mesoporous silicas in the presence of $H_2O$ involve flowing $CO_2$ over a sample that has been pre-equilibrated with $H_2O$ and measuring the increase in weight. To calculate the $CO_2$ uptake, it is assumed that the amount of $H_2O$ adsorbed is unaffected by $CO_2$ adsorption. Recent binary adsorption measurements, however, have shown that this assumption often leads to incorrect conclusions about the amount of $CO_2$ adsorbed in the presence of $H_2O$.[67]

Many of the amine-functionalized silicas investigated for $CO_2$ capture have been based on MCM-41 (Mobil composition of matter no. 41), which consists of cylindrical mesopores that are arranged in a hexagonal lattice.[68] In this work, three amine-functionalized derivatives of MCM-41 were synthesized according to previous reports: 3-aminopropyl grafted MCM-41 (1°-MCM-41), 3-methylaminopropyl grafted MCM-41 (2°-MCM-41), and polyethylenimine impregnated MCM-41 (PEI-MCM-41).[69,70b] Based on elemental analysis, 4.2 mmol of 1° amine per g silica and 3.7 mmol of 2° amine per g silica were grafted in 1°-MCM-41 and 2°-MCM-41, respectively, which is comparable to the average loading for all reported monoamine-appended silicas of just over 3 mmol/g.[11a] At 40 °C and 1 bar, both 1°-MCM-41 and 2°-MCM-41 adsorb nearly 0.5 molecules of $CO_2$ per amine, as expected for ammonium carbamate formation under dry conditions (Figure 11).

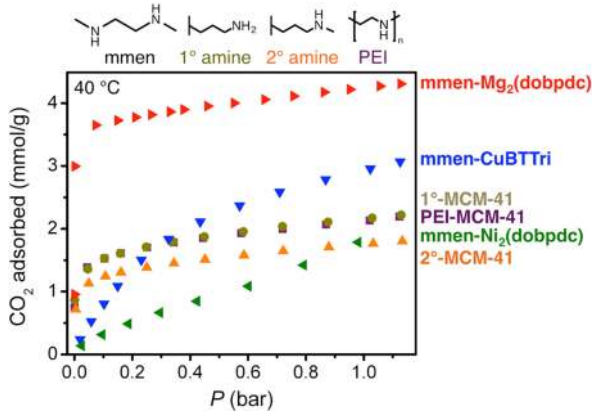


**Figure 11.** Pure $CO_2$ adsorption isotherms at 40 °C for metal−organic frameworks and mesoporous silicas that feature alkylamine groups.

With 33% of N by mass and a roughly 1:1:1 mixture 1°, 2°, and 3° amines, branched PEI has a high density of amine groups and has been shown to have improved $CO_2$ capture performance when it is impregnated inside a solid support rather than neat.[70] The PEI-MCM-41 sample synthesized in this work contained 32 wt % of PEI (7.4 mmol N per g silica). At 40 °C and 1 bar, PEI-MCM-41 adsorbs 0.28 molecules of $CO_2$ per amine (2.1 mmol/g), which is consistent with the


DOI: 10.1021/jacs.5b00838
J. Am. Chem. Soc. 2015, 137, 4787−4803

amine efficiencies of previously reported amine-impregnated silicas (Figure 11).[11]

Here, multicomponent experiments were used to measure directly the amount of $CO_2$ adsorbed from a mixture of $CO_2$, $N_2$, and $H_2O$ at 40 °C and a $CO_2$ partial pressure near 0.15 bar. Note that since primary amines are prone to deactivate by forming urea linkages under dry conditions,[69] the pure $CO_2$ and multicomponent isotherms reported here were measured on separate samples. At an equilibrium $H_2O$ partial pressure of 19 mbar (26% RH), the amount of $CO_2$ adsorbed by 1°-MCM-41 decreased by 25%. This result appears to be in conflict with an earlier report that used a thermogravimetric analyzer coupled to a mass spectrometer to show a 76% increase in $CO_2$ adsorption for 1°-MCM-41 at 24 mbar of $H_2O$ and 25 °C.[67] The two 1°-MCM-41 samples have nearly identical amine loadings, but the bare MCM-41 silica used in this work has an average pore size of 2.4 nm, while the previously reported material used a pore-enlarged variant of MCM-41 with an average pore size of nearly 11 nm.[71] The different pore sizes of the resulting amine-grafted materials could be responsible for the different $CO_2$ capacities observed under humid conditions.

The amount of $CO_2$ adsorbed by 2°-MCM-41 at 17 mbar of $H_2O$ was within error of the dry $CO_2$ uptake, suggesting that no bicarbonate was formed. Although the sample was equilibrated for over 24 h, it is likely that bicarbonate formation is exceedingly slow in this secondary amine material and equilibrium was not reached over the course of the multicomponent measurement.[66] During the multicomponent measurement, the total pressure of the system was still decreasing at a very slow rate even after 24 h of forced equilibration, which suggests that some $CO_2$ adsorption was still occurring with very slow kinetics. There are several literature reports of constant $CO_2$ uptake for amine-appended silicas under both dry and humid conditions, but whether or not kinetics are a factor in these experiments is uncertain.[11a]

In contrast to 1°-MCM-41 and 2°-MCM-41, the amount of $CO_2$ adsorbed in PEI-MCM-41 increased significantly from 1.5 mmol/g (0.20 $CO_2$ per N) to 2.5(1) mmol/g (0.34 $CO_2$ per N) at 17 mbar of $H_2O$. This 67(7)% increase is slightly higher than the 40% increase observed for 50 wt % PEI-MCM-41 in a dynamic breakthrough experiment at 75 °C.[70c] Although the observed $CO_2$ capacity is <1 $CO_2$ per amine, it is possible that either bicarbonate is still forming but the $CO_2$ partial pressure is not high enough to reach a full capacity of 1 $CO_2$ per amine or that not all of the amine sites of the PEI are accessible to $CO_2$.

**Amine-Appended Metal–Organic Frameworks.** While initial efforts to functionalize solid adsorbents with amines involved mostly mesoporous silicas, several amine-appended metal–organic frameworks have recently shown promising $CO_2$ capture properties.[72] For instance, the amine-appended metal–organic framework $H_3[(Cu_4Cl)_3(BTTri)_8(mmen)_{12}]$ (mmen-CuBTTri; $H_3$BTTri =1,3,5-tri(1*H*-1,2,3-triazol-4-yl)-benzene) features diamines that are coordinated to the exposed $Cu^{2+}$ cations of its sodalite-type cages (Figure 1), resulting in a nearly 250% increase in the amount of $CO_2$ adsorbed at 0.15 bar and 25 °C as compared to the bare framework.[72c] Similar to 1°-MCM-41, mmen-CuBTTri shows a very slight decrease in $CO_2$ uptake in the presence of $N_2$ and $H_2O$, but still adsorbs 0.9(2) mmol/g of $CO_2$ (Table S3). This demonstrates that appending amines to exposed metal cation sites in metal–organic frameworks is a viable strategy for adsorbing $CO_2$ under humid conditions.

In contrast to mesoporous silicas, highly crystalline metal–organic frameworks offer the advantage of well-defined and ordered sites for attaching amines, a feature that was recently shown to lead to unprecedented cooperative $CO_2$ binding and low $CO_2$ capture regeneration energies in the diamine-appended metal–organic framework mmen-$Mg_2$(dobpdc).[73] In this material, which features an expanded version of $Mg_2$(dobdc), one end of each diamine is attached to an exposed $Mg^{2+}$ cation, while the other end is exposed on the surface (Figure 1). With all diamines spaced exactly 6.8 Å apart along each hexagonal channel, the density of amine groups in mmen-$Mg_2$(dobpdc) is 7.3 mmol/mL, exceeding that of a 30 wt % monoethanolamine solution (4.9 mmol/mL).

At 40 °C and pressures below 0.5 mbar, the mechanism for $CO_2$ adsorption in mmen-$Mg_2$(dobpdc) is thought to be similar to that of classical amine-appended silicas: two free amine groups react with a $CO_2$ molecule to form ammonium carbamate (Figure 12). At higher pressures, however, there is a sharp step in the $CO_2$ adsorption isotherm of mmen-$Mg_2$(dobpdc), and both ends of the diamine begin to participate in $CO_2$ binding. Specifically, a proton is transferred from a metal-bound amine to a neighboring free amine as $CO_2$ simultaneously inserts into the Mg–N bond, resulting in the formation of one-dimensional chains of ammonium carbamate that run parallel to each chain of $Mg^{2+}$ cations.[73] This insertion-based $CO_2$ adsorption mechanism leads to strong, cooperative $CO_2$ binding, and at 0.15 bar and 40 °C, one $CO_2$ molecule is adsorbed per mmen to give a total capacity of 3.73 mmol/g (14.1 wt %).

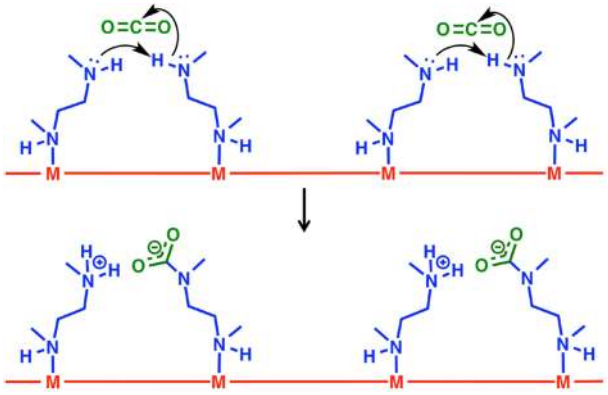


**Figure 12.** Proposed mechanism for $CO_2$ adsorption in mmen-$Ni_2$(dobpdc) and pre-step $CO_2$ adsorption in mmen-$Mg_2$(dobpdc) is shown at four neighboring M-mmen sites within an infinite one-dimensional chain of such sites running along the crystallographic *c* axis of the compound. Simultaneous proton transfer and nucleophilic attack of an uncoordinated amine on a $CO_2$ molecule forms an ammonium carbamate species.

Since $CO_2$, but not $N_2$ or $H_2O$, induces a phase transition in mmen-$Mg_2$(dobpdc), changing both the structure and composition of the adsorbent, it is impossible to use pure-component adsorption isotherms to predict $CO_2$ selectivity and capacity for a mixture of $CO_2$, $N_2$, and $H_2O$. Instead, the direct measurement of multicomponent adsorption is the only way to investigate the effects of $H_2O$ and $N_2$ on $CO_2$ binding in mmen-$Mg_2$(dobpdc) at equilibrium. Of particular interest is to determine whether the insertion-based $CO_2$ adsorption mechanism is affected by $H_2O$ and if ammonium carbamate is still the only form of adsorbed $CO_2$ under humid conditions.


DOI: 10.1021/jacs.5b00838
J. Am. Chem. Soc. 2015, 137, 4787–4803

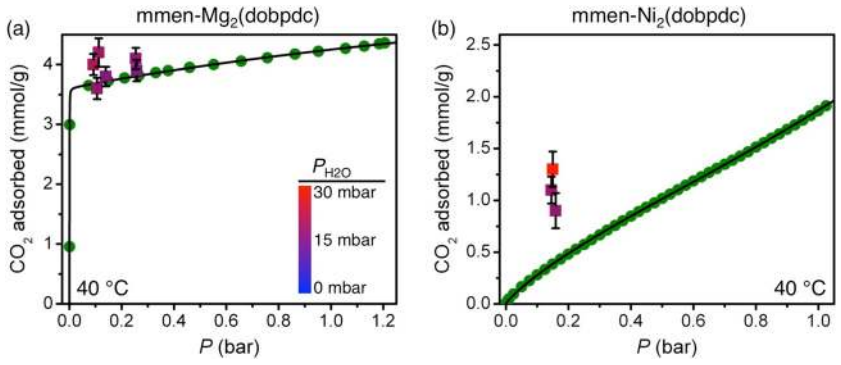


**Figure 13.** A summary of $CO_2$, $N_2$, $H_2O$ multicomponent equilibrium measurements at 40 °C for (a) mmen-$Mg_2$(dobpdc) and (b) mmen-$Ni_2$(dobdc). Green circles represent pure $CO_2$ adsorption isotherms for each compound, and black lines are the corresponding dual-site Langmuir fits. Square data points represent the amount of $CO_2$ adsorbed from a mixture of $CO_2$, $N_2$, and $H_2O$, and the color of the square indicates the equilibrium partial pressure of $H_2O$. The exact values of $P_{H_2O}$ can be found in Table S3.

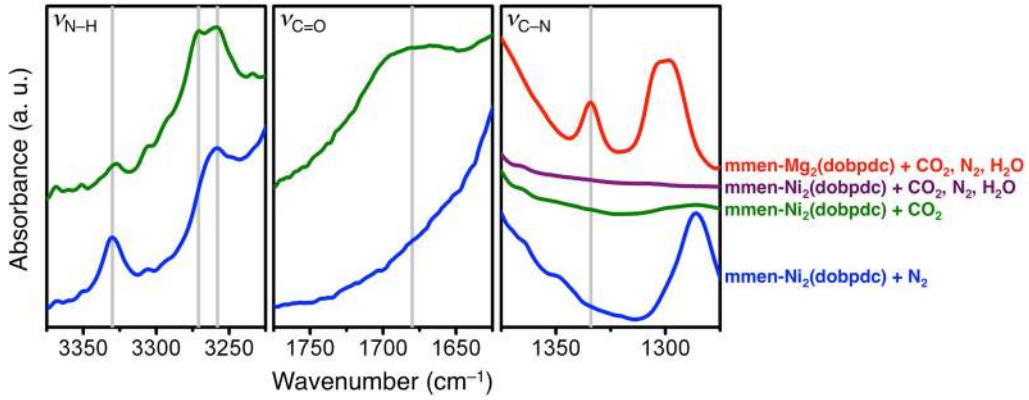


**Figure 14.** Infrared spectra upon dosing activated mmen-$Ni_2$(dobpdc) with $N_2$ (blue), $CO_2$ (green), and a mixture of $CO_2$, $N_2$, and $H_2O$ (purple), and dosing activated mmen-$Mg_2$(dobpdc) with a mixture of $CO_2$, $N_2$, and $H_2O$ (red) at 25 °C. The three different regions show bands corresponding to N–H, C=O, and C–N stretching vibrations, from left to right, respectively.

Significantly, multicomponent measurements with $H_2O$ partial pressures as high as 19 mbar, $CO_2$ partial pressures between 100 and 300 mbar, and $N_2$ partial pressures between 500 and 700 mbar, clearly show that the amount of $CO_2$ adsorbed from a mixture of $CO_2$, $N_2$, and $H_2O$ is the same as, or slightly higher than, from pure $CO_2$. Thus, $H_2O$ and $N_2$ do not have a significant effect on $CO_2$ adsorption in mmen-$Mg_2$(dobpdc) (Figure 13a). To the best of our knowledge, the multicomponent $CO_2$ uptake of 4.2(2) mmol/g (15.6 wt %) for mmen-$Mg_2$(dobpdc) represents the highest value ever reported for any metal–organic framework or silica under similar humid conditions. While no $N_2$ adsorption is observed in mmen-$Mg_2$(dobpdc) during the multicomponent experiments, between 4.9 and 9.5 mmol/g of $H_2O$ is adsorbed, depending on the exact equilibrium conditions. Since $CO_2$ and $H_2O$ do not compete for the same binding sites, it should be possible to reduce this $H_2O$ adsorption without affecting the amount of $CO_2$ adsorbed by, for instance, tuning the alkylamine or bridging organic ligand to increase the hydrophobicity of the pore surface. Note that one of the multicomponent measurements was repeated four further times on the same sample with identical results after regenerating at 100 °C under vacuum for 2 h, demonstrating that $CO_2$ and $H_2O$ adsorption is fully reversible (Figure 5). Longer cycling studies with mixtures of $CO_2$, $N_2$, and $H_2O$ and regeneration using a pure temperature swing are currently in progress.

To confirm that $CO_2$ insertion into the Mg–N bond is still occurring in the presence of $H_2O$, infrared spectroscopy measurements were performed after equilibrating a sample of mmen-$Mg_2$(dobpdc) with a mixture of $CO_2$, $N_2$, and $H_2O$ (Figure 14). Previously, a sharp band was observed at 1334 $cm^{-1}$ in the infrared spectrum of mmen-$Mg_2$(dobpdc) dosed with pure $CO_2$. This band was assigned to the C–N stretch of a carbamate and is only present after insertion of $CO_2$ into the M–N bond generates an O-bound carbamate species with more double-bond character in the C–N bond.[73] Significantly, there is also a sharp band observed at 1334 $cm^{-1}$ for mmen-$Mg_2$(dobpdc) in the presence of $CO_2$, $N_2$, and $H_2O$, confirming that $CO_2$ insertion into the M–N bond is still occurring and that $H_2O$ does not change the mechanism for $CO_2$ adsorption (Figure 14). Although the multicomponent measurements indicate a very slight increase in the amount of $CO_2$ adsorbed in the presence of $H_2O$, there is no evidence of any carbonate or bicarbonate species in the infrared spectrum.

In the isostructural nickel analogue of this framework, mmen-$Ni_2$(dobpdc), the increased strength of the Ni–N bond makes the insertion of $CO_2$ thermodynamically unfavorable, and the $CO_2$ adsorption isotherms do not contain a step, resulting in just 0.4 mmol/g (1.7 wt %) of $CO_2$ adsorbed at 40 °C and 0.15 bar.[73] Note that while the pure $CO_2$ isotherm of mmen-$Ni_2$(dobpdc) is not nearly as steep as expected for an adsorbent with strong $CO_2$ binding sites, the isosteric heat of adsorption at low coverage is still −40 to −60 kJ/mol. The isotherm is not


DOI: 10.1021/jacs.5b00838
J. Am. Chem. Soc. 2015, 137, 4787–4803

as steep as that of most metal−organic frameworks with $CO_2$ binding energies in this range, such as $Mg_2$(dobdc), because the entropy of $CO_2$ adsorption is much more positive in mmen-$Ni_2$(dobpdc) than in more classical materials.[73] This strong $CO_2$ binding and large entropy of adsorption can likely be explained by a similar mechanism as for the pre-step adsorption in mmen-$Mg_2$(dobpdc): a proton is transferred between the free ends of two neighboring diamines and $CO_2$ is bound via the formation of ammonium carbamate, resulting in one $CO_2$ bound per every two mmen (Figure 12). In order for this proton transfer to occur, the diamines likely lose some rotational degrees of freedom as ammonium carbamate pairs are formed, which leads to the large entropy penalty associated with $CO_2$ binding.

To support the proposed mechanism for dry $CO_2$ adsorption in mmen-$Ni_2$(dobpdc), infrared spectroscopy measurements were performed on mmen-$Ni_2$(dobpdc) in the presence of pure $N_2$ and pure $CO_2$ (Figure 14). Under a pure $N_2$ atmosphere, two distinct N−H vibrations are observed at 3330 and 3258 $cm^{-1}$ and can be assigned to the free and Ni-bound ends of the diamines, respectively. The metal-bound N−H stretch is identical to that observed for mmen-$Mg_2$(dobpdc), while the free N−H stretch is red-shifted by 4 $cm^{-1}$.[73] Upon exposure to 1 bar of pure $CO_2$, the free N−H resonance at 3330 $cm^{-1}$ disappears, and a new vibration is observed at 3271 $cm^{-1}$. The disappearance of the free N−H vibration is consistent with the formation of ammonium. If only the free ends of each diamine participate in the reaction with $CO_2$, then half of all diamines would be expected to have an ammonium on the free end, while the other half of diamines would have a carbamate (Figure 12). Indeed, there are two N−H resonances of roughly equal intensity observed at 3271 and 3258 $cm^{-1}$ in the presence of $CO_2$ that can be assigned to the N−H on Ni-bound ends of diamines that have either an ammonium or a carbamate on the free end. A broad feature also grows in at roughly 1680 $cm^{-1}$ after $CO_2$ dosing, which is consistent with the C═O vibration of carbamate. Finally, no new bands are observed between 1275 and 1375 $cm^{-1}$ after $CO_2$ adsorption, which is consistent with the ammonium carbamate reaction occurring at the free ends of the diamines, with no insertion of $CO_2$ into the M−Ni bond.

Somewhat unexpectedly, the amount of $CO_2$ adsorbed in mmen-$Ni_2$(dobpdc) increases nearly 3-fold to 1.3(2) mmol/g (5.4 wt %) in the presence of 29 mbar of $H_2O$ and 691 mbar of $N_2$ (Figure 13b). This substantial increase in $CO_2$ adsorption is greater than typically observed for amine-appended silicas and suggests that $H_2O$ has a strong effect on the $CO_2$ binding mechanism. Despite the large increase in $CO_2$ uptake, only 0.37(7) mmol of $CO_2$ is adsorbed per mmol of free amine under the multicomponent conditions.

To gain further insight into these multicomponent results, infrared spectroscopy measurements were also performed for mmen-$Ni_2$(dobpdc) under an atmosphere of $N_2$, $CO_2$, and $H_2O$ (Figure 14). Unfortunately, a very broad and high intensity band above 3000 $cm^{-1}$, resulting from the large amount of $H_2O$ in the gas-phase, overwhelms any N−H resonances (Figures S18, S19). Still, no new bands are observed between 1275 and 1375 $cm^{-1}$, demonstrating that $CO_2$ insertion into the M−Ni bond does not occur in mmen-$Ni_2$(dobpdc) even in the presence of $H_2O$. Although $CO_2$ insertion is ruled out, the infrared spectrum of mmen-$Ni_2$(dobpdc) does not provide any conclusive evidence that can explain the increased $CO_2$ uptake in the presence of $H_2O$. It is possible that bicarbonate is formed, but its infrared bands are masked by $H_2O$ or the organic bridging ligand. Alternatively, $H_2O$ may facilitate the formation of more ammonium carbamate at lower $CO_2$ partial pressures by, for instance, breaking up hydrogen-bonding between neighboring diamines to expose more $CO_2$ binding sites than are present under dry conditions.[65g]

## CONCLUSIONS

The multicomponent results reported in this work for adsorption of $CO_2$, $N_2$, and $H_2O$ in 15 different materials, including metal−organic frameworks, zeolites, mesoporous silicas, and an activated carbon, are summarized in Figure 15.

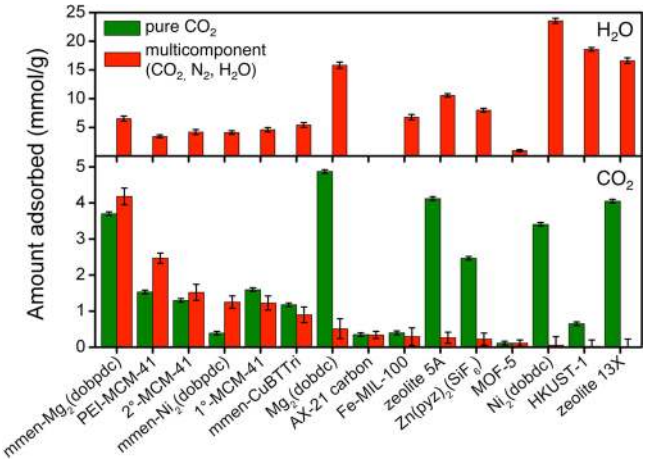


**Figure 15.** A summary of the multicomponent adsorption measurements performed in this work for mixtures of $CO_2$, $N_2$, and $H_2O$ at 40 °C and equilibrium conditions representative of a coal-fired power plant flue gas. The green bars represent the amount of $CO_2$ adsorbed in a single-component isotherm at the same $CO_2$ partial pressure as the multicomponent experiment. The red bars in the bottom pane represent the amount of $CO_2$ adsorbed in the multicomponent experiment. The red bars in the upper pane represent the amount of $H_2O$ adsorbed in the multicomponent experiment. For the multicomponent experiments, all partial pressures of $N_2$ are between 679 and 698 mbar, of $CO_2$ are between 113 and 178 mbar, and of $H_2O$ are between 10 and 29 mbar. Total pressures are between 821 and 890 mbar. See Table S3 for exact equilibrium partial pressures and amounts adsorbed. Error bars are shown at a 95% confidence interval.

Here, a multicomponent data point is plotted for each material at the equilibrium conditions most representative of the composition of a coal-fired power plant flue gas. In the bottom pane of the bar graph, the amount of $CO_2$ adsorbed from the multicomponent mixture of $CO_2$, $N_2$, and $H_2O$ (red) is compared to the amount of $CO_2$ adsorbed at the same partial pressure in the absence of $N_2$ and $H_2O$ (green). In the top pane, the amount of $H_2O$ adsorbed in the multicomponent experiment is shown. As has been discussed in detail, all of the adsorbents with exposed metal cations or anions take up a significant amount of $H_2O$ and negligible amount of $CO_2$ under these simulated flue gas equilibrium conditions, while MOF-5 and the AX-21 activated carbon have mostly nonpolar surfaces that lead not only to very little $H_2O$ adsorption but also to very little $CO_2$ uptake at these low pressures. Adsorbents functionalized with alkylamines, however, maintain a significant $CO_2$ capacity at the multicomponent equilibrium conditions, with mmen-$Mg_2$(dobpdc) adsorbing a record amount of $CO_2$ in the presence of $H_2O$.


DOI: 10.1021/jacs.5b00838
J. Am. Chem. Soc. 2015, 137, 4787−4803

In addition to maximizing $CO_2$ adsorption, minimizing $H_2O$ adsorption is critical to achieving low regeneration energies in any $CO_2$ capture process that involves a temperature swing since some of the heat supplied to desorb $CO_2$ will also go toward desorbing $H_2O$. The direct measurement of equilibrium $H_2O$ adsorption in the presence of $N_2$ and $CO_2$ is thus important for identifying adsorbents with the best $CO_2$ capture performance. This is particularly true for adsorbents that change upon binding $CO_2$, where $H_2O$ adsorption may be very different before and after $CO_2$ adsorption. It is worth noting that measuring the amount of $H_2O$ adsorbed in a breakthrough experiment with $CO_2$ is extremely challenging, if not impossible, when the column is pre-equilibrated with $H_2O$, as is often necessary when running small-scale breakthrough experiments.

Although the multicomponent results presented in this work targeted equilibrium conditions representative of adsorption from a post-combustion flue gas, evaluating multicomponent equilibria at desorption conditions is also important. Since a pure temperature swing or vacuum-assisted temperature swing process will likely be most effective for $CO_2$ capture,[8,12c] evaluating the amount of $CO_2$ and $H_2O$ adsorbed from mixtures as a function of regeneration temperature and pressure is necessary to determine $CO_2$ and $H_2O$ working capacities and to calculate regeneration energies. Recently, it was shown that the cooperative $CO_2$ binding in mmen-$Mg_2$(dobpdc) allows a $CO_2$ working capacity of nearly 14 wt % (3.7 mmol/g) to be achieved with an unprecedented temperature swing of just 50 °C.[73] The effects of $H_2O$ on this working capacity are currently being investigated under both dynamic and equilibrium conditions. Because of their structural and chemical tunability, metal−organic frameworks functionalized with alkylamines are a particularly promising class of solid adsorbents for achieving high $CO_2$ working capacities, minimal $H_2O$ adsorption, and low regeneration energies at post-combustion $CO_2$ capture conditions.

In addition to $CO_2$, $N_2$, and $H_2O$, multicomponent measurements and long-term cycling studies that include other flue gas components, such as $O_2$, $NO_x$, and $SO_x$, will be valuable in assessing adsorbents for $CO_2$ capture applications. Measuring multicomponent equilibrium kinetics and heats of adsorption, which are particularly challenging experiments, is also important but rarely reported in the literature for gas mixtures.[17b] While no real $CO_2$ capture process will operate under true equilibrium conditions, equilibrium data are essential for comparing different materials and for simulating the dynamic processes of a large-scale separation.

## ■ ASSOCIATED CONTENT

### Supporting Information

Experimental details, surface area measurements, additional adsorption isotherms, descriptions of isotherm fitting, multicomponent calculations, multicomponent error analysis, and complete multicomponent data set. This material is available free of charge via the Internet at http://pubs.acs.org.

## ■ AUTHOR INFORMATION


### Corresponding Author

*jrlong@berkeley.edu

### Present Addresses

[§]School of Chemical and Biomedical Engineering and Singapore Membrane Technology Center, Nanyang Technological University, Singapore.

[⊥]Institute for Integrated Cell-Material-Sciences, Kyoto University, Kyoto, Japan.

[‖]Mosaic Materials, Inc., Berkeley, CA 94720, United States.


### Notes

The authors declare no competing financial interest.

## ■ ACKNOWLEDGMENTS

This research was funded by the Advanced Research Projects Agency − Energy (ARPA-E), U.S. Department of Energy. We thank Adam Berger, Dr. Abhoyjit Bhown, Prof. Berend Smit, Prof. Rajamani Krishna, Dr. Zoey Herm, Dr. Eric Bloch, and Dianne Xiao for helpful discussions, and David Gygi and Henry Jiang for assisting with sample preparation. We also thank Fulbright New Zealand for partial support of K.S., NSF for providing partial graduate fellowship support for J.A.M and J.E.B, and Chevron for providing partial graduate fellowship support for J.A.M.

## ■ REFERENCES


(1) *$CO_2$ Emissions from Fuel Combustion* , International Energy Agency (IEA): Paris, 2014. DOI: 10.1787/co2_fuel-2014-en.

(2) In *Climate Change 2013: The Physical Science Basis. Contribution of Working Group I to the Fifth Assessment Report of the Intergovernmental Panel on Climate Change*; Stocker, T. F. et al.; Cambridge University Press: New York, 2013.

(3) (a) Chu, S. *Science* **2009**, *325*, 1599. (b) Haszeldine, R. S. *Science* **2009**, *325*, 1647.

(4) (a) Wheeler, D.; Ummel, K. *Calculating CARMA: Global Estimation of $CO_2$ Emissions from the Power Sector*; Center for Global Development: Washington, DC, 2008; Working Paper 145. (b) Ummel, K. *CARMA Revisited: An Updated Database of Carbon Dioxide Emissions from Power Plants Worldwide*; Center for Global Development: Washington, DC, 2012; Working Paper 304.

(5) Fout, T.; Murphy, J. T. *DOE/NETL's Carbon Capture R&D Program for Existing Coal-Fired Power Plants*; National Energy Technology Laboratory: Pittsburgh, PA, 2009; DOE/NETL 2009/1356.

(6) Figueroa, J. D.; Fout, T.; Plasynski, S.; McIlvried, H.; Srivastava, R. D. *Int. J. Greenhouse Gas Control* **2008**, *2*, 9.

(7) (a) Bhown, A. S. *Energy Procedia* **2014**, *63*, 542. (b) Boot-Handford, M. E.; Abanades, J. C.; Anthony, E. J.; Blunt, M. J.; Brandani, S.; Mac Dowell, N.; Fernández, J. R.; Ferrari, M.-C.; Gross, R.; Hallet, J. P.; Haszeldine, R. S.; Heptonstall, P.; Lyngfelt, A.; Makuch, Z.; Mangano, E.; Porter, R. T. J.; Pourkashanian, M.; Rochelle, G. T.; Shah, N.; Yao, J. G.; Fennell, P. S. *Energy Envrion. Sci.* **2014**, *7*, 130.

(8) Drage, T. C.; Snape, C. E.; Stevens, L. A.; Wood, J.; Wang, J.; Cooper, A. I.; Dawson, R.; Guo, X.; Satterley, C.; Irons, R. *J. Mater. Chem.* **2012**, *22*, 2815.

(9) The $H_2O$ content of a coal-fired power plant's flue gas is highly dependent on whether or not a wet or dry flue gas desulphurization (FGD) process is in use.

(10) Rochelle, G. T. *Science* **2009**, *325*, 1652.

(11) (a) Choi, S.; Drese, J. H.; Jones, C. W. *ChemSusChem* **2009**, *2*, 796. (b) D'Alessandro, D. M.; Smit, B.; Long, J. R. *Angew. Chem., Int. Ed.* **2010**, *49*, 6058. (c) Wang, Q.; Luo, J.; Zhong, Z.; Borgna, A. *Energy Environ. Sci.* **2011**, *4*, 42. (d) Sumida, K.; Rogow, D. L.; Mason, J. A.; McDonald, T. M.; Bloch, E. D.; Herm, Z. R.; Bae, T.-H.; Long, J. R. *Chem. Rev.* **2012**, *112*, 724. (e) Liu, Y.; Wang, Z. U.; Zhou, H.-C. *Greenhouse Gasses Sci. Technol.* **2012**, *2*, 239. (f) Liu, J.; Thallapally, P. K.; McGrail, B. P.; Brown, D. R.; Liu, J. *Chem. Soc. Rev.* **2012**, *41*,




DOI: 10.1021/jacs.5b00838
*J. Am. Chem. Soc.* 2015, 137, 4787−4803

2308.9. (g) Zhang, Z.; Yao, Z.-Z.; Xiang, S.; Chen, B. *Energy Environ. Sci.* **2014**, *7*, 2868.
(12) (a) Yazaydin, A. Ö.; Snurr, R. Q.; Park, T.-H.; Koh, K.; Liu, J.; LeVan, M. D.; Benin, A. I.; Jakubczak, P.; Lanuza, M.; Galloway, D. B.; Low, J. J.; Willis, R. R. *J. Am. Chem. Soc.* **2009**, *131*, 18198. (b) Mason, J. A.; Sumida, K.; Herm, Z. R.; Krishna, R.; Long, J. R. *Energy Environ. Sci.* **2011**, *4*, 3030. (c) Lin, L.-C.; Berger, A. H.; Martin, R. L.; Kim, J.; Swisher, J. A.; Jariwala, K.; Rycroft, C. H.; Bhown, A. S.; Deem, M. W.; Haranczyk, M.; Smit, B. *Nat. Mater.* **2012**, *11*, 633.
(13) Wang, J.; Ryan, D.; Anthony, E. J.; Wildgust, N.; Aiken, T. *Energy Procedia* **2011**, *4*, 3071.
(14) Keskin, S.; van Heest, T. M.; Sholl, D. S. *ChemSusChem* **2010**, *3*, 879.
(15) (a) Babarao, R.; Jiang, J. *Energy Environ. Sci.* **2009**, *2*, 1088. (b) Ding, L.; Yazaydin, A. Ö. *J. Phys. Chem. C* **2012**, *116*, 22987. (c) Yu, K.; Kiesling, K.; Schmidt, J. R. *J. Phys. Chem. C* **2012**, *116*, 20480. (d) Yu, J.; Ma, Y.; Balbuena, P. B. *Langmuir* **2012**, *28*, 8064. (e) Huang, H.; Zhang, W.; Liu, D.; Zhong, C. *Ind. Eng. Chem. Res.* **2012**, *51*, 10031. (f) Babarao, R.; Jiang, Y.; Medhekar, N. V. *J. Phys. Chem. C* **2013**, *113*, 26976. (g) Yu, J.; Balbuena, P. B. *J. Phys. Chem. C* **2013**, *117*, 3383. (h) Liu, Y.; Liu, J.; Lin, Y. S.; Chang, M. *J. Phys. Chem. C* **2014**, *118*, 6744.
(16) (a) Liang, Z.; Marshall, M.; Chaffee, A. L. *Energy Fuels* **2009**, *23*, 2785. (b) Yazaydin, A. Ö.; Benin, A. I.; Faheem, S. A.; Jakubczak, P.; Low, J. J.; Willis, R. R.; Snurr, R. Q. *Chem. Mater.* **2009**, *21*, 1425. (c) Liu, J.; Wang, Y.; Benin, A. I.; Jakubczak, P.; Willis, R. R.; LeVan, M. D. *Langmuir* **2010**, *26*, 14301. (d) Liu, J.; Benin, A. I.; Furtado, A. M. B.; Jakubczak, P.; Willis, R. R.; LeVan, M. D. *Langmuir* **2011**, *27*, 11451. (e) Kizzie, A. C.; Wong-Foy, A. G.; Matzger, A. J. *Langmuir* **2011**, *27*, 6368. (f) Han, S.; Huang, Y.; Watanabe, T.; Dai, Y.; Walton, K.; Nair, S.; Sholl, D. S.; Meredith, J. C. *ACS Comb. Sci.* **2012**, *14*, 263. (g) Han, S.; Huang, Y.; Watanabe, T.; Nair, S.; Walton, K. S.; Sholl, D. S.; Meredith, J. C. *Microporous Mesoporous Mater.* **2013**, *173*, 86. (h) Yang, Q.; Vaesen, S.; Ragon, F.; Wiersum, A. D.; Wu, D.; Lago, A.; Devic, T.; Martineau, C.; Taulelle, F.; Llewellyn, P. L.; Jobic, H.; Zhong, C.; Serre, C.; Weireld, G. D.; Maurin, G. *Angew. Chem., Int. Ed.* **2013**, *51*, 1. (i) Woodward, R. T.; Stevens, L. A.; Dawson, R.; Vijayaraghavan, M.; Hasell, T.; Silverwood, I. P.; Ewing, A. V.; Ratvijivech, T.; Exley, J. D.; Chong, S. Y.; Blanc, F.; Adams, D. J.; Kazarian, S. G.; Snape, C. E.; Drage, T. C.; Cooper, A. I. *J. Am. Chem. Soc.* **2014**, *136*, 9028. (j) Bae, Y.-S.; Liu, J.; Wilmer, C. E.; Sun, H.; Dickey, A. N.; Kim, M. B.; Benin, A. I.; Willis, R. R.; Barpaga, D.; LeVan, M. D.; Snurr, R. Q. *Chem. Commun.* **2014**, *50*, 3296. (k) Burtch, N. C.; Jasuja, H.; Walson, K. S. *Chem. Rev.* **2014**, *114*, 10575.
(17) (a) Sircar, S. *Ind. Eng. Chem. Res.* **2006**, *45*, 5435. (b) Sircar, S. *Ind. Eng. Chem. Res.* **2007**, *46*, 2917. (c) Broom, D. P.; Thomas, K. M. *MRS Bull.* **2013**, *38*, 412.
(18) Myers, A. L.; Prausnitz, J. M. *AIChE J.* **1965**, *11*, 121.
(19) (a) Krishna, R.; van Baten, J. M. *Chem. Eng. J.* **2007**, *133*, 121. (b) Krishna, R.; van Baten, J. M. *Phys. Chem. Chem. Phys.* **2011**, *13*, 10593.
(20) Siperstein, F. R.; Myers, A. L. *AIChE J.* **2001**, *47*, 1141.
(21) Talu, O. *Chem. Ing. Technol.* **2011**, *83*, 67.
(22) Talu, O. *Adv. Colloid Interface Sci.* **1998**, *76*−*77*, 227.
(23) Examples for $CO_2$, $N_2$, $H_2O$ breakthrough experiments in metal−organic frameworks include: (a) Zhao, Y.; Yao, K. X.; Teng, B.; Zhang, T.; Han, Y. *Energy Environ. Sci.* **2013**, *6*, 3684. (b) Liu, Q.; Ning, L.; Zheng, S.; Tao, M.; Shi, Y.; He, Y. *Sci. Rep.* **2013**, *3*, 2916. (c) Li, D.; Furukawa, H.; Deng, H.; Liu, C.; Yaghi, O. M.; Eisenberg, D. S. *Proc. Natl. Acad. Sci. U.S.A.* **2014**, *111*, 191. (d) Nguyen, N. T. T.; Furukawa, H.; Gándara, F.; Nguyen, H. T.; Cordova, K. E.; Yaghi, O. M. *Angew. Chem., Int. Ed.* **2014**, *53*, 1.
(24) Li, G.; Xiao, P.; Webley, P.; Zhang, J.; Singh, R.; Marshall, M. *Adsorption* **2008**, *14*, 415.
(25) Pirngruber, G. D.; Hamon, L.; Bourrelly, S.; Llewellyn, P. L.; Lenoir, E.; Guillerm, V.; Serre, C.; Devic, T. *ChemSusChem* **2012**, *5*, 762.
(26) (a) Rajendran, A.; Kariwala, V.; Farooq, S. *Chem. Eng. Sci.* **2008**, *63*, 2696. (b) Hofman, P. S.; Rufford, T. E.; Chan, K. I.; May, E. F. *Adsorption* **2012**, *18*, 251.
(27) Pigorini, G.; LeVan, M. D. *Ind. Eng. Chem. Res.* **1998**, *37*, 2516.
(28) Fletcher, A. J.; Benham, M. J.; Thomas, K. M. *J. Phys. Chem. B* **2002**, *106*, 7474.
(29) (a) Hamon, L.; Frère, M.; Weireld, G. D. *Adsorption* **2008**, *14*, 493. (b) Watson, G. C.; Jensen, N. K.; Rufford, T. E.; Chan, K. I.; May, E. F. *J. Chem. Eng. Data* **2012**, *57*, 93.
(30) Ding, Y.; LeVan, M. D. *Rev. Sci. Instrum.* **2002**, *73*, 230.
(31) Brandani, F.; Ruthven, D. M. *Ind. Eng. Chem. Res.* **2003**, *42*, 1462.
(32) Talu, O.; Zwiebel, I. *AIChE J.* **1986**, *32*, 1263.
(33) (a) Rege, S. U.; Yang, R. T. *Chem. Eng. Sci.* **2001**, *56*, 3781. (b) Cai, B.-C.; Han, Q.-J.; Tang, L.-J.; Zhang, Y.; Yu, R.-Q. *Ind. Eng. Chem. Res.* **2008**, *47*, 6835. (c) Ohlin, L.; Bazin, P.; Thibault-Starzyk, F.; Hedlund, J.; Grahn, M. *J. Phys. Chem. C* **2013**, *117*, 16972.
(34) Rynders, R. M.; Rao, M. B.; Sircar, S. *AIChE J.* **1997**, *43*, 2456.
(35) Note that the multicomponent results reported here should not be dependent on the exact dosing procedure used to achieve a given set of equilibrium conditions, provided $H_2O$ adsorption is fully reversible. All $H_2O$ gas dosing was preformed in small steps relative to the total amount of $H_2O$ adsorbed by a sample so as to minimize any potential effects from hysteresis in $H_2O$ adsorption.
(36) (a) Li, H.; Eddaoudi, M.; O'Keeffe, M.; Yaghi, O. M. *Nature* **1999**, *402*, 276. (b) Millward, A. R.; Yaghi, O. M. *J. Am. Chem. Soc.* **2005**, *127*, 17998. (c) Kaye, S. S.; Dailly, A.; Yaghi, O. M.; Long, J. R. *J. Am. Chem. Soc.* **2007**, *129*, 14176. (d) Walton, K. S.; Millward, A. R.; Dubbeldam, D.; Frost, H.; Low, J. J.; Yaghi, O. M.; Snurr, R. Q. *J. Am. Chem. Soc.* **2008**, *130*, 406.
(37) Otowa, T.; Tanibata, R.; Itoh, M. *Gas Sep. Purif.* **1993**, *7*, 241.
(38) Sircar, S.; Golden, T. C.; Rao, M. B. *Carbon* **1996**, *34*, 1.
(39) Hao, G.-P.; Li, W.-C.; Qian, D.; Wang, G.-H.; Zhang, W.-P.; Zhang, T.; Wang, A.-Q.; Schüth, F.; Bongard, H.-J.; Lu, A.-H. *J. Am. Chem. Soc.* **2011**, *133*, 11378.
(40) Barton, S. S.; Evans, M. J. B.; MacDonald, J. A. F. *Carbon* **1991**, *29*, 1099.
(41) Dubinin, M. M.; Zaverina, E. D.; Serpinsky, V. V. *J. Chem. Soc.* **1955**, 1760.
(42) Angell, C. L. *J. Phys. Chem.* **1966**, *70*, 2420.
(43) Caskey, S. R.; Wong-Foy, A. G.; Matzger, A. J. *J. Am. Chem. Soc.* **2008**, *130*, 10870.
(44) (a) Lee, J.-S.; Kim, J.-H.; Kim, J.-T.; Suh, J.-K.; Lee, J.-M.; Lee, C.-H. *J. Chem. Eng. Data* **2002**, *47*, 1237. (b) Wang, Y.; LeVan, M. D. *J. Chem. Eng. Data* **2009**, *54*, 2839. (c) Bae, T.-H.; Hudson, M. R.; Mason, J. A.; Queen, W. L.; Dutton, J. J.; Sumida, K.; Micklash, K. J.; Kaye, S. S.; Brown, C. M.; Long, J. R. *Energy Environ. Sci.* **2013**, *6*, 128.
(45) (a) Rosi, N. L.; Kim, J.; Eddaoudi, M.; Chen, B.; O'Keeffe, M.; Yaghi, O. M. *J. Am. Chem. Soc.* **2005**, *127*, 1504. (b) Dietzel, P. D. C.; Blom, R.; Fjellvåg, H. *Eur. J. Inorg. Chem.* **2008**, 3624.
(46) Dietzel, P. D. C.; Panella, B.; Hirscher, M.; Blom, R.; Fjellvåg, H. *Chem. Commun.* **2006**, 959.
(47) Chui, S. S. Y.; Lo, S. M. F.; Charmant, J. P. H.; Orpen, A. G.; Williams, I. D. *Science* **1999**, *283*, 1148.
(48) Horcajada, P.; Surblé, S.; Serre, C.; Hong, D.-Y.; Seo, Y.-K.; Chang, J.-S.; Grenèche, J.-M.; Margiolaki, I.; Férey, G. *Chem. Commun.* **2007**, 2820.
(49) (a) Adams, J. M.; Haselden, D. A.; Hewat, A. W. *J. Solid State Chem.* **1982**, *44*, 245. (b) Adams, J. M.; Haselden, D. A. *J. Solid State Chem.* **1984**, *51*, 83.
(50) Olson, D. H. *Zeolites* **1995**, *15*, 439.
(51) (a) Britt, D.; Furukawa, H.; Wang, B.; Glover, T. G.; Yaghi, O. M. *Proc. Natl. Acad. Sci. U.S.A.* **2009**, *106*, 20637. (b) Dietzel, P. D. C.; Besikiotis, V.; Blom, R. *J. Mater. Chem.* **2009**, *19*, 7362. (c) Wu, H.; Simmons, J. M.; Srinivas, G.; Zhou, W.; Yildirim, T. *J. Phys. Chem. Lett.* **2010**, *1*, 1946. (d) Valenzano, L.; Civalleri, B.; Chavan, S.; Palomino, G. T.; Areán, C. O.; Bordiga, S. *J. Phys. Chem. C* **2010**, *114*, 11185. (e) Bao, Z.; Yu, L.; Ren, Q.; Lu, X.; Deng, S. *J. Colloid Interface Sci.* **2011**, *353*, 549.


DOI: 10.1021/jacs.5b00838
*J. Am. Chem. Soc.* 2015, 137, 4787−4803

(52) (a) Huang, H.; Zhang, W.; Liu, D.; Zhong, C. *Ind. Eng. Chem. Res.* **2012**, *51*, 10031. (b) Yu, J.; Balbuena, P. B. *J. Phys. Chem. C* **2013**, *113*, 3383. (c) Joos, L.; Swisher, J. A.; Smit, B. *Langmuir* **2013**, *29*, 15936. (d) Lin, L.-C.; Lee, K.; Gagliardi, L.; Neaton, J. B.; Smit, B. *J. Chem. Theory Comput.* **2014**, *10*, 1477.
(53) (a) Brandani, F.; Ruthven, D. M. *Ind. Eng. Chem. Res.* **2004**, *43*, 8339. (b) Wang, Y.; Levan, M. D. *J. Chem. Eng. Data* **2010**, *55*, 3189.
(54) Liu, J.; Tian, J.; Thallapally, P. K.; McGrail, P. B. *J. Phys. Chem. C* **2012**, *116*, 9575.
(55) Hudson, M. R.; Queen, W. L.; Mason, J. A.; Fickel, D. W.; Lobo, R. F.; Brown, C. M. *J. Am. Chem. Soc.* **2012**, *134*, 1970.
(56) Wang, Q. M.; Shen, D.; Bülow, M.; Lau, M. L.; Deng, S.; Fitch, F. R.; Lemcoff, N. O.; Semanscin, J. *Microporous Mesoporous Mater.* **2002**, *55*, 217.
(57) Wuttke, S.; Bazin, P.; Vimont, A.; Serre, C.; Seo, Y.-K.; Hwang, Y. K.; Chang, J.-S.; Férey, G.; Daturi, M. *Chem.—Eur. J.* **2012**, *18*, 11959.
(58) Soubeyrand-Lenoir, E.; Vagner, C.; Yoon, J. W.; Bazin, P.; Ragon, F.; Hwang, Y. K.; Serre, C.; Chang, J.-S.; Llewellyn, P. L. *J. Am. Chem. Soc.* **2012**, *134*, 10174.
(59) (a) Nugent, P.; Belmabkhout, Y.; Burd, S. D.; Cairns, A. J.; Luebke, R.; Forrest, K.; Pham, T.; Ma, S.; Space, B.; Wojtas, L.; Eddaoudi, M.; Zaworotko, M. J. *Nature* **2013**, *495*, 80. (b) Noro, S.; Hijikata, Y.; Inukai, M.; Fukushima, T.; Horike, S.; Higuchi, M.; Kitagawa, S.; Akutagawa, T.; Nakamura, T. *Inorg. Chem.* **2013**, *52*, 280. (c) Shekhah, O.; Belmabkhout, Y.; Chen, Z.; Guillerm, V.; Cairns, A.; Adil, K.; Eddaoudi, M. *Nat. Commun.* **2014**, *5*, 4228.
(60) Uemura, K.; Maeda, A.; Maji, T. K.; Kanoo, P.; Kita, H. *Eur. J. Inorg. Chem.* **2009**, *16*, 2329.
(61) (a) Veawab, A.; Tontiwachwuthikul, P.; Chakma, A. *Ind. Eng. Chem. Res.* **1999**, *38*, 3917. (b) Bontemps, D.; Chopin, F.; Le Moullec, Y.; Morand, T.; Zanella, Y.; Pinto, C. *Energy Procedia* **2014**, *63*, 787.
(62) (a) Caplow, M. *J. Am. Chem. Soc.* **1968**, *90*, 6795. (b) Danon, A.; Stair, P. C.; Weitz, E. *J. Phys. Chem. C* **2011**, *115*, 11540.
(63) Leal, O.; Bolívar, C.; Ovalles, C.; García, J. J.; Espidel, Y. *Inorg. Chim. Acta* **1995**, *240*, 183.
(64) Bollini, P.; Didas, S. A.; Jones, C. W. *J. Mater. Chem.* **2011**, *21*, 15100.
(65) (a) Huang, H. Y.; Yang, R. T.; Chinn, D.; Munson, C. L. *Ind. Eng. Chem. Res.* **2003**, *42*, 2427. (b) Chang, A. C. C.; Chuang, S. S. C.; Gray, M.; Soong, Y. *Energy Fuels* **2003**, *17*, 468. (c) Hiyoshi, N.; Yogo, K.; Yashima, T. *Microporous Mesoporous Mater.* **2005**, *84*, 357. (d) Khatri, R. A.; Chuang, S. S. C.; Soong, Y.; Gray, M. *Energy Fuels* **2006**, *20*, 1514. (e) Harlick, P. J. E.; Sayari, A. *Ind. Eng. Chem. Res.* **2007**, *46*, 446. (f) Brunelli, N. A.; Didas, S. A.; Venkatasubbaiah, K.; Jones, C. W. *J. Am. Chem. Soc.* **2012**, *134*, 13950. (g) Didas, S. A.; Sakwa-Novak, M. A.; Foo, G. S.; Sievers, C.; Jones, C. W. *J. Phys. Chem. Lett.* **2014**, *5*, 4194.
(66) (a) Vaidya, P. D.; Kenig, E. *Chem. Eng. Technol.* **2007**, *30*, 1467. (b) Serna-Guerrero, R.; Belmabkhout, Y.; Sayari, A. *Chem. Eng. J.* **2010**, *158*, 513.
(67) Serna-Guerrero, R.; Da'na, E.; Sayari, A. *Ind. Eng. Chem. Res.* **2008**, *47*, 9406.
(68) Kresge, C. T.; Leonowicz, M. E.; Roth, W. J.; Vartuli, J. C.; Beck, J. S. *Nature* **1992**, *359*, 710.
(69) Sayari, A.; Belmabkhout, Y.; Da'na, E. *Langmuir* **2012**, *28*, 4241.
(70) (a) Satyapal, S.; Filburn, T.; Trela, J.; Strange, J. *Energy Fuels* **2001**, *15*, 250. (b) Xu, X.; Song, C.; Andresen, J. M.; Miller, B. G.; Scaroni, A. W. *Energy Fuels* **2002**, *16*, 1463. (c) Xu, X.; Song, C.; Miller, B. G.; Scaroni, A. W. *Ind. Eng. Chem. Res.* **2005**, *44*, 8113. (d) Xu, X.; Song, C.; Miller, B. G.; Scaroni, A. W. *Fuel Process. Technol.* **2005**, *86*, 1457.
(71) Sayari, A.; Yang, Y.; Kruk, M.; Jaroniec, M. *J. Phys. Chem. B* **1999**, *103*, 3651.
(72) (a) Hwang, Y. K.; Hong, D.-Y.; Chang, J.-S.; Jhung, S. H.; Seo, Y.-K.; Kim, J.; Vimont, A.; Daturi, M.; Serre, C.; Férey, G. *Angew. Chem., Int. Ed.* **2008**, *47*, 4144. (b) Demessence, A.; D'Alessandro, D. M.; Foo, M. L.; Long, J. R. *J. Am. Chem. Soc.* **2009**, *131*, 8784. (c) McDonald, T. M.; D'Alessandro, D. M.; Krishna, R.; Long, J. R. *Chem. Sci.* **2011**, *2*, 2022. (d) Montoro, C.; García, E.; Calero, S.; Pérez-Fernández, M. A.; López, A. L.; Barea, E.; Navarro, J. A. R. *J. Mater. Chem.* **2012**, *22*, 10155. (e) McDonald, T. M.; Lee, W. R.; Mason, J. A.; Wiers, B. M.; Hong, C. S.; Long, J. R. *J. Am. Chem. Soc.* **2012**, *134*, 7056. (f) Choi, S.; Watanabe, T.; Sholl, D. S.; Jones, C. W. *J. Phys. Chem. Lett.* **2012**, *3*, 1136. (g) Lu, W.; Sculley, J. P.; Yuan, D.; Krishna, R.; Zhou, H.-C. *J. Phys. Chem. C* **2013**, *117*, 4057. (h) Lee, W. R.; Hwang, S. Y.; Ryu, D. W.; Lim, K. S.; Han, S. S.; Moon, D.; Choi, J.; Hong, C. S. *Energy Environ. Sci.* **2014**, *7*, 744. (i) Fracaroli, A. M.; Furukawa, H.; Suzuki, M.; Dodd, M.; Okajima, S.; Gándara, F.; Reimer, J. A.; Yaghi, O. M. *J. Am. Chem. Soc.* **2014**, *136*, 8863.
(73) McDonald, T. M.; Mason, J. A.; Kong, X.; Bloch, E. D.; Gygi, D.; Dani, A.; Crocellà, V.; Giordanino, F.; Odoh, S. O.; Drisdell, W.; Vlaisavljevich, B.; Dzubak, A. L.; Poloni, R.; Schnell, S. K.; Planas, N.; Lee, K.; Pascal, T.; Wan, L. F.; Prendergast, D.; Neaton, J. B.; Smit, B.; Kortright, J. B.; Gagliardi, L.; Bordiga, S.; Reimer, J. A.; Long, J. R. *Nature* **2015**, *519*, 303.


DOI: 10.1021/jacs.5b00838
*J. Am. Chem. Soc.* 2015, 137, 4787−4803